

1 ***Streptococcus pyogenes Cas9 ribonucleoprotein delivery for efficient, rapid and***  
2 ***marker-free gene editing in Trypanosoma and Leishmania***

4 Running title: **Efficient delivery of Cas9 in kinetoplastids**

6 Asencio Corinne<sup>1\*</sup>, Hervé Perrine<sup>1\*</sup>, Morand Pauline<sup>1</sup>, Oliveres Quentin<sup>1</sup>, Morel Chloé  
7 Alexandra<sup>1</sup>, Prouzet-Mauleon Valérie<sup>2</sup>, Biran Marc<sup>3</sup>, Monic Sarah<sup>1</sup>, Bonhivers Mélanie<sup>1</sup>,  
8 Robinson Derrick Roy<sup>1</sup>, Ouellette Marc<sup>4</sup>, Rivière Loïc<sup>1</sup>, Bringaud Frédéric<sup>1</sup> and Tetaud  
9 Emmanuel<sup>1#</sup>

11 <sup>1</sup>Univ. Bordeaux, CNRS, MFP, UMR 5234, F-33000, Bordeaux, France

13 <sup>2</sup>Univ. Bordeaux, CNRS/INSERM, TBMCore/CRISP'edit, UAR 3427/US005, F-33000,  
14 Bordeaux, France.

16 <sup>3</sup>Univ. Bordeaux, CNRS, CRMSB, UMR 5536, F-33000, Bordeaux, France

18 <sup>4</sup>Centre de Recherche en Infectiologie du Centre de Recherche du CHU de Québec and  
19 Département de Microbiologie, Infectiologie et Immunologie, Faculté de Médecine,  
20 Université Laval, Québec, Québec, Canada.

22 \*Co-first authors

23

24 #Corresponding author: [Emmanuel.tetaud@u-bordeaux.fr](mailto:Emmanuel.tetaud@u-bordeaux.fr)

25 **SUMMARY**

26 Kinetoplastids are unicellular eukaryotic flagellated parasites found in a wide range of hosts  
27 within the animal and plant kingdoms. They are known to be responsible in humans for  
28 African sleeping sickness (*Trypanosoma brucei*), Chagas disease (*Trypanosoma cruzi*), and  
29 various forms of leishmaniasis (*Leishmania* spp.), as well as several animal diseases with  
30 important economic impact (African trypanosomes, including *T. congolense*).  
31 Understanding the biology of these parasites necessarily implies the ability to manipulate  
32 their genomes. In this study, we demonstrate that transfection of a ribonucleoprotein  
33 complex, composed of recombinant *Streptococcus pyogenes* Cas9 (*SpCas9*) and an *in*  
34 *vitro*-synthesized guide RNA, results in rapid and efficient genetic modifications of  
35 trypanosomatids, in marker-free conditions. This approach was successfully developed to  
36 inactivate, delete and mutate candidate genes in various stages of the life cycle of *T. brucei*  
37 and *T. congolense*, and *Leishmania* promastigotes. The functionality of *SpCas9* in these  
38 parasites now provides, to the research community working on these parasites, a rapid  
39 and efficient method of genome editing, without requiring plasmid construction and  
40 selection by antibiotics. Importantly, this approach is adaptable to any wild-type parasite,  
41 including field isolates.

42

43 **KEYWORDS**

44 • CRISPR/Cas9  
45 • Marker-free  
46 • Kinetoplastids  
47 • Protist  
48 • Efficiency  
49 • Universal  
50 • Ribonucleoprotein complex transfection

51

52 **INTRODUCTION**

53 In the realm of modern molecular biology, few innovations have captured the world's  
54 attention like CRISPR-Cas9. The CRISPR-Cas9 system has catapulted molecular biology  
55 into a new era of precision gene editing and genetic engineering. CRISPR (Clustered  
56 Regularly Interspaced Short Palindromic Repeats) and CRISPR-associated protein 9  
57 (CRISPR-Cas9) is a revolutionary genome-editing technology that has unlocked  
58 unprecedented opportunities for precise manipulation of the genetic code. Since its  
59 discovery in the early 2000s (Mojica et al., 2005, Barrangou et al., 2007), CRISPR-Cas9  
60 has rapidly evolved into a game-changing tool with the potential to transform medicine,  
61 agriculture, biotechnology, and various other fields (Jinek et al., 2012). This  
62 groundbreaking system is derived from a remarkable natural defense mechanism found in  
63 bacteria and archaea, allowing researchers to edit, correct, or modify genes with an  
64 accuracy and efficiency that was previously unimaginable (Ishino et al., 1987, Mojica et  
65 al., 2005, Barrangou et al., 2007).

66 Obviously, this technology was very quickly used to study trypanosomatids, which are  
67 unicellular eukaryotic flagellate parasites that affect millions of people and animals  
68 worldwide. In humans, they are responsible for African sleeping sickness (Human African  
69 trypanosomiasis), Chagas disease (American trypanosomiasis), and leishmaniasis in South  
70 America, Africa, India, the Mediterranean region and the Middle East. African Animal  
71 Trypanosomiasis, including Nagana, are debilitating diseases affecting livestock, primarily  
72 cattle in sub-Saharan Africa. Nagana, which is caused by *Trypanosoma congolense*,  
73 *Trypanosoma vivax* and *Trypanosoma brucei brucei*, leads to severe health issues,  
74 including anemia, weight loss, and decreased productivity in infected animals, making it a  
75 significant economic and agricultural concern in affected regions (Desquesnes et al., 2022).  
76 Understanding the biology of these parasites necessarily requires the ability to manipulate  
77 their genomes. Before the development of the CRISPR-Cas9 system, genome modification  
78 was achieved through homologous recombination with resistance markers for selection, or  
79 by RNA interference, but only in *T. brucei* (Ngo et al., 1998) and *T. congolense* (Inoue et  
80 al., 2002, Coustou et al., 2012) as *T. cruzi* and *Leishmania* spp do not share the RNA  
81 interference machinery (Kolev et al., 2011). Because of genome diploidy,  
82 deletion/inactivation of genes proved to be time-consuming and conditioned by the limited  
83 number of available antibiotic resistance markers.

84 The CRISPR-Cas9 system has been now employed to modify the genomes of *T. brucei*, *T.*  
85 *cruzi* and *Leishmania* spp. with a rapidly growing number of publications (founding articles  
86 are : (Peng et al., 2014, Sollelisis et al., 2015, Zhang and Matlashewski, 2015, Zhang et al.,  
87 2017, Lander et al., 2015, Lander et al., 2016, Lander et al., 2017, Beneke et al., 2017,  
88 Rico et al., 2018, Shaw et al., 2020, Kovarova et al., 2022). In most studies, Cas9 or Cas9-  
89 gRNA complexes are endogenously expressed after transfection of the parasites and

90 selection with antibiotic resistance markers. However, the CRISPR-Cas9 system still has  
91 some shortcomings, such as the impact of constitutive Cas9 expression, which result in  
92 genome instability (Zhang et al., 2017, Boutin et al., 2021) and can lead to a decrease in  
93 cell growth (Ryan et al., 2014, Peng et al., 2014). Conditional expression of Cas9, as  
94 described in *T. brucei*, is helpful to overcome this issue (Rico et al., 2018, Kovarova et al.,  
95 2022). Another issue with the CRISPR-Cas9 system is the potential off-target genome  
96 disruption (Fu et al., 2013). The ongoing development of new, increasingly accurate Cas9  
97 variants, should also limit this problem. Interestingly, CRISPR-mediated editing can be  
98 achieved by transfecting cells with *in vitro*-generated Cas9 protein/guide RNA complexes.  
99 As recombinant Cas9 is rapidly eliminated after transfection, this approach, which limits  
100 potential off-target (D'Astolfo et al., 2015) and reduces toxicity issues (Kim et al., 2014,  
101 Liang et al., 2015), has proven to be particularly efficient in *T. cruzi* and *Plasmodium*  
102 (Soares Medeiros et al., 2017, Crawford et al., 2017). This method is straightforward, fast,  
103 and highly efficient, as it does not require gene cloning and minimizes the use of selection  
104 markers. However, in *T. cruzi*, *Leishmania* spp. and *T. brucei*, this approach relies  
105 exclusively on the use of a smaller Cas9, isolated from *Staphylococcus aureus* (SaCas9)  
106 (Soares Medeiros et al., 2017). The same authors also reported that Cas9 isolated from  
107 *Streptococcus pyogenes* (SpCas9), despite being the most commonly used and  
108 commercialized, does not function in these parasites, and the lack of activity appears to  
109 be due to the larger size of SpCas9 compared to SaCas9, which is approximately 40 kDa  
110 smaller (Soares Medeiros et al., 2017).

111  
112 In this study, we have demonstrated that SpCas9 is fully functional after transfection of  
113 the Cas9/gRNA complex in both the bloodstream (BSF) and procyclic (PCF) forms of *T.*  
114 *brucei* and *T. congolense*, as well as in the promastigotes of *Leishmania infantum*. This  
115 Cas9/gRNA complex can be delivered into cells, with or without a repair sequence, to  
116 inactivate, mutate, or tag candidate genes, without the need for selection markers and  
117 with very high efficiency. The functionality of SpCas9 in these parasites now provides the  
118 research community working on these parasites a rapid and efficient method for genome  
119 edition without requiring gene cloning and/or selection, that only requires cloning of  
120 modified cell lines. It will also allow genome editing of cells that are difficult to cultivate or  
121 whose cell density is too low to envisage using conventional techniques, such as field  
122 isolates. Finally, this approach should be adaptable to all kinetoplastids and, importantly,  
123 any transfectable cell type.

124

125 **RESULTS**

126 **The size of the *SpCas9*/RNP complex has no detectible impact on genome editing**  
127 **activity**

128 Soares Medeiros *et al.* described in *T. cruzi*, *T. brucei* and *Leishmania* the unexpected result  
129 that exogenous ribonucleoprotein Cas9 from *Streptococcus pyogenes* (*SpCas9*, 163 kDa)  
130 was not functional after transfection, in contrast to the smaller *Staphylococcus aureus* Cas9  
131 (*SaCas9*, 124 kDa) (Soares Medeiros *et al.*, 2017). Since *SpCas9* is fully active when  
132 endogenously expressed (Peng *et al.*, 2014), it was proposed that ribonucleoprotein  
133 *SpCas9* complexes are not internalized by electroporation in trypanosomatids. To revisit  
134 these data, we tried to inactivate a constitutively expressed cytosolic GFP in *T. brucei* PCF  
135 using extracellular RNP complexes composed of *SpCas9* and guide RNAs (gRNAs). We used  
136 the commercial *SpCas9* from Integrated DNA Technologies (IDT, *SpCas9* nuclease V3) and  
137 three gRNAs targeting different sequences of the *GFP* gene (**Table 1**). GFP expression was  
138 monitored by flow cytometry at 24, 48, 72, and 144 h post-transfection with the RNP  
139 complexes (**Figure 1A**).  $5 \times 10^5$  GFP-expressing *T. brucei* PCF cells were subjected to  
140 electroporation with 20 µg of gRNA-loaded *SpCas9* (GFP1, 2 or 3), or gRNA only as a  
141 control (GFP2). Unexpectedly, transfection of GFP-expressing PCF without *SpCas9* (**Figure**  
142 **1A - Top left panel**) resulted in a very strong drop in fluorescence after 24 h for about  
143 50% of the population, probably related to the electroporation conditions. However, 48 h  
144 later, GFP expression recovered to its initial level (**Figure 1A - Top left panel**).  
145 Importantly, a strong decrease in fluorescence occurred immediately after transfection  
146 with GFP1, GFP2 and GFP3 gRNA-loaded *SpCas9*, which did not recover to its initial level  
147 after 72 h (**Figure 1A - gRNA GFP1, GFP2 and GFP3**), indicating that a significant  
148 portion of cells do not express active GFP anymore. It is noteworthy that GFP1 and GFP2  
149 gRNA are more efficient at inactivating GFP expression than GFP3 gRNA (**Figure 1A - Bar**  
150 **chart**) and the efficiency depends on the amount of RNP complex transfected (1.5-fold  
151 increase of GFP-negative cells with a 3-fold increase of GFP2 gRNA-loaded *SpCas9*)  
152 (**Figure 1A - Bar chart**).

153 To confirm that the decrease in GFP expression is indeed caused by Cas9/gRNA-dependent  
154 GFP gene inactivation, we cell-sorted and cloned cells failing to express GFP and sequenced  
155 the DNA region targeted by the GFP2 guide RNA used (**Figure 1C**). As expected, a 33-bp  
156 deletion at the gRNA targeting site was observed in all GFP-negative cells (**Figure 1C**).  
157 The deleted region is flanked by two 8-bp homologous sequences, which suggests a repair  
158 of double-strand breaks by the microhomology-mediated end-joining (MMEJ) pathway as  
159 previously described in *T. cruzi* and *Leishmania* (Peng *et al.*, 2014, Zhang *et al.*, 2017).  
160 These data show that the commercial *SpCas9* from IDT is fully functional in our  
161 experimental protocols and suggest that the size of the exogenous ribonucleoprotein  
162 complex is not a limiting factor, contrary to the hypothesis made for *T. cruzi*. The only

163 difference that we could identify between the IDT *SpCas9* and the one used by Soares  
164 Medeiros *et al.* is the number of nuclear localization signals (NLS), three *versus* two,  
165 suggesting that the lack of activity in *T. cruzi* could be explained by weak nuclear targeting  
166 of the complex after transfection.

167 In order to produce our own in-house recombinant Cas9 protein, we constructed a  
168 recombinant DNA *SpCas9* sequence (e*SpCas9*, a rationally engineered Cas9 with improved  
169 specificity (Slaymaker *et al.*, 2016)) containing three NLS regions, *i.e.*, one at the N-  
170 terminus and two at the C-terminus of the protein, plus two polyhistidine tracts to allow  
171 the purification of the expressed recombinant protein by chromatography (**Figure 1B**).  
172 The protein was expressed and purified in *E. coli* (Cf. Experimental procedures, **Figure S1**)  
173 and its activity was assayed by replacing the IDT *SpCas9* with the e*SpCas9* in the GFP2  
174 gRNA/Cas9 complex. As expected, the purified e*SpCas9* is able to dose-dependently  
175 inactivate GFP expression (**Figure 1B**). Note that above 40 µg of e*SpCas9*, there is no  
176 further decrease in GFP expression (**Figure 1B, right**). Sequencing of the *GFP* gene in  
177 cloned cell lines confirmed the inactivation of the gene by a 33-bp deletion. A larger 97-bp  
178 deletion flanked by two 6-bp homologous regions was also detected in clone Bc3 (**Figure**  
179 **1C**). It is worth noting that the presence of polyhistidine tracts, one each at the N and C-  
180 terminal of the protein, does not appear to affect Cas9 activity. We concluded that the  
181 edition of PCF *T. brucei* genes with *SpCas9*/gRNA complexes is functional and the use of  
182 laboratory-produced e*SpCas9* is equally effective as the commercial *SpCas9* (IDT).  
183

#### 184 **Development of a marker-free approach for editing the genomes of *T. brucei* PCF 185 and BSF**

186 Cas9-mediated double-strand DNA breaks can be repaired by homology-directed repair  
187 (HDR), as long as an appropriate repair template is provided (Peng *et al.*, 2014). We have  
188 tested this by inactivating the *TbFis1* gene (Tb927.10.8660), in both *T. brucei* PCF and BSF  
189 using marker-dependent and marker-free approaches. *TbFis1* protein is a potential  
190 homologue of the mitochondrial fission factor identified in yeast, Fis1p (Mozdy *et al.*, 2000),  
191 which enables the recruitment of the dynamin Dnm1 to the mitochondria and triggers  
192 mitochondrial fission. The first approach consists of inserting a repair template encoding a  
193 resistance gene (in this case against phleomycin, *BleR*) flanked by 5' and 3' regulatory  
194 sequences and a short homology region of the *TbFis1* gene flanking the Cas9-cleavage site  
195 (50 bp) (**Figure 2A**). Cells were cloned after 8 to 12 days of culture in the presence of  
196 phleomycin. The correct insertion of the repair DNA fragment was controlled by PCR and  
197 sequencing, as shown in **Figure 2B/C**. After Cas9-mediated recombination, the size of the  
198 targeted *TbFis1* gene increased by 880 bp, which corresponds to the size of the repair  
199 cassette (**Figure 2B**). Both alleles encoding *TbFis1* (homozygotes) were targeted in 100%

200 of PCF clones but in only 10% of BSF clones (**Figure 2B**). The 90% remaining BSF clones  
201 had a single allele inactivated (heterozygotes) (**Table 1**).  
202 The second approach consists of inserting a shorter repair cassette composed of stop  
203 codons in all three reading frames and a restriction site absent in the targeted gene (here  
204 *BamHI*), flanked by short regions of homology corresponding to 50-bp flanking the Cas9-  
205 cleavage site (**Figure 2A - SBS**). The *BamHI* restriction site enables rapid discrimination  
206 of repair template integration on one or two alleles after PCR and digestion with *BamHI*.  
207 Under these marker-free conditions, cells were cloned one to three days after transfection  
208 and insertion of the repair cassette was tested by PCR/*BamHI* digestion and sequencing  
209 (**Figure 2B - SBS**). 3% and 4% of the BSF clones tested were inactivated on both alleles  
210 or one allele only, respectively (**Table 1**). Obtaining a large number of homozygous  
211 mutants confirms that the *TbFis1* gene is not essential for PCF and BSF growth.  
212 Incidentally, the inactivation of the *TbFis1* gene did not induce a change in mitochondrial  
213 structure (**Figure S2**).  
214

### 215 **Inactivation of a *T. brucei* multigene family by SpCas9**

216 Genetic manipulation of trypanosomatids is often made difficult when high number of  
217 resistance markers are required, as exemplified for sequential inactivation of several genes  
218 or when multigene families are addressed (Reis-Cunha et al., 2018). We therefore tested  
219 whether transfection, with the gRNA/RNP complex, is also effective for the inactivation of  
220 a multigene family, here the one encoding glycerol kinase (GK) in *T. brucei* PCF. RNAi-  
221 mediated down-regulation of GK expression has shown that, in standard growth conditions,  
222 this non-essential gene family is required to metabolize glycerol in *T. brucei* PCF and BSF  
223 (Pineda et al., 2018, Allmann et al., 2021). GK is encoded by eleven tandemly-arranged  
224 copies distributed over the two alleles, containing five and six copies, respectively (**Figure**  
225 **S2**). We tested a single gRNA targeting the entire multigenic family and a repair cassette  
226 including the phleomycin resistance marker (*BleR*) (**Figure 3A**). The fate of the allelic *GK*  
227 gene clusters after transfection and selection with phleomycin was tested by PCR using  
228 primers flanking the Cas9 recognition site. All the tested phleomycin-resistant clones  
229 (eleven clones) showed the presence of a single ~1,500-bp band corresponding to the  
230 parental allele (616 bp) inactivated by insertion of the repair cassette (880 bp), suggesting  
231 that *GK* genes are inactivated (**Figure 3B, Table 1**). This was confirmed by a Southern-  
232 blot analysis with the *GK* probe after digestion of the genomic DNA with a restriction  
233 enzyme present once in each of the *GK* repeat unit (*KpnI*), which generated a 5,197-bp  
234 band corresponding to the *GK* copy located at the 5' extremity of both allelic clusters (two  
235 copies) plus an intense 3,582-bp band corresponding to the other *GK* genes (nine copies)  
236 (**Figure 3A/C**). As expected, the genome of all the tested mutant cell lines contains two  
237 *KpnI* bands-containing *GK* whose size is increased by ~800 bp, corresponding to the length

238 of the repair cassette. It is noteworthy that, following cleavage by Cas9 in the same locus,  
239 it is likely that several *GK* copies were deleted by homologous recombination. Indeed, a  
240 Southern blot analysis of genomic DNA digested by *Mfe*I (which is absent in the *GK* repeat  
241 units), revealed a significant reduction of the size of one *GK* allelic cluster in the 1B10, 2G2  
242 and 2F11 clones (**Figure S3**). As expected, a western blot analysis with the anti-*GK*  
243 immune serum showed that *GK* expression is abolished in all the analyzed mutant cell  
244 lines, confirming that they are *bona fide* *GK* null mutants (*GK*<sup>-/-</sup>) (**Figure 3D**). In addition,  
245 glycerol metabolism is abolished in the *GK*<sup>-/-</sup> cell lines, as shown by quantitative proton  
246 NMR spectrometry analyses of the <sup>13</sup>C-enriched end products excreted from the  
247 metabolism of uniformly <sup>13</sup>C-enriched glycerol ([U-<sup>13</sup>C]-glycerol) (Bringaud et al., 2015,  
248 Pineda et al., 2018, Allmann et al., 2021). Indeed, the parental PCF *T. brucei* convert [U-  
249 <sup>13</sup>C]-glucose or [U-<sup>13</sup>C]-glycerol to <sup>13</sup>C-enriched acetate and succinate. In contrast, the  
250 excretion of <sup>13</sup>C-enriched end products from [U-<sup>13</sup>C]-glycerol is abolished in the *GK*<sup>-/-</sup> 2E6  
251 cell line, while the metabolism of [U-<sup>13</sup>C]-glucose is unaffected (**Figure 3E**). Taken  
252 together, these data demonstrate the high efficiency of a single transfection with  
253 gRNA/*SpCas9* complexes to inactivate all copies of a large multigene family.

254

### 255 ***SpCas9* is also functional in other trypanosomatids**

256 We also tested the efficiency of RNP complex delivery to edit the genome of the  
257 promastigote forms of *Leishmania infantum* and of the bloodstream and procyclic forms of  
258 *Trypanosoma congolense*. Several approaches have been used to inactivate the gene  
259 encoding ALDH, the mitochondrial enzyme responsible for converting acetaldehyde to  
260 acetate in *L. infantum* promastigotes (LINF\_250017300, ALDH, manuscript in preparation),  
261 using an *SpCas9*/gRNA complex targeting the ALDH sequence and various repair cassettes.  
262 Here we used repair cassettes to insert (i) a puromycin resistance marker (*PacR*), (ii) a  
263 fluorescent protein (monomeric RED, mRED) and (iii) a short sequence containing stop  
264 codons and a *Bam*HI restriction site (SBS) as described above (**Figure 4A**). After  
265 transfection, clones were selected either by addition of puromycin (*PacR* cassette, ALDH<sup>-/-</sup>  
266 PAC cells), by cell cytometry at 595/613 nm (mRED cassette, ALDH<sup>-/-</sup> mRED cells) or by  
267 PCR and sequencing after cell cloning (SBS cassette, ALDH<sup>-/-</sup> SBS cells). In each condition,  
268 the insertion of the repair cassette was checked by PCR with primers flanking the insertion  
269 site (**Figure 4A/B**). We were able to obtain homozygous mutant clones for each repair  
270 cassette, with efficiencies ranging from 30% (ALDH<sup>-/-</sup> SBS cells) to 83% (ALDH<sup>-/-</sup> mRED  
271 cells) (**Table 1**). It should be noted that the *PacR* and mRED cassettes are only composed  
272 of the corresponding ORF inserted in frame with the ALDH coding sequence (**Figure 4A**).  
273 The mRED protein showed a mitochondrial-like pattern by immunofluorescence in the  
274 ALDH<sup>-/-</sup> mRED cell line, as opposed to the cytosolic-like pattern observed for mRED  
275 expressed with an expression vector, which suggests that the N-terminal mitochondrial

276 targeting motif of ALDH targeted the chimeric ALDH/mRED protein to the mitochondrion  
277 (**Figure 4C**). To confirm that both *ALDH* alleles were indeed inactivated, we quantified the  
278 product of the ALDH enzymatic reaction, *i.e.*, acetate, which is excreted in the medium  
279 from the metabolism of threonine. As expected, production of  $^{13}\text{C}$ -enriched acetate is  
280 abolished in the  $\text{ALDH}^{-/-}$  PAC clone 1B1, as shown by proton NMR spectrometry analysis of  
281 the  $^{13}\text{C}$ -enriched end products excreted from the metabolism of [U- $^{13}\text{C}$ ]-threonine (**Figure**  
282 **4D**) (Bringaud et al., 2015). Integrating an ectopic copy of the *ALDH* encoding gene in an  
283  $\text{ALDH}^{-/-}$  PAC cell line restored  $^{13}\text{C}$ -enriched acetate production from the metabolism of [U-  
284  $^{13}\text{C}$ ]-threonine, as opposed to expression of GFP (**Figure 4D**). Similarly, the  $\text{ALDH}^{-/-}$  *SBS*  
285 mutant (clone A1) no longer excretes  $^{13}\text{C}$ -enriched acetate from the metabolism of [U-  
286  $^{13}\text{C}$ ]-threonine (**Figure 4D**).

287 To test this approach in *T. congolense*, we targeted the *LysoPLA* gene  
288 (TcIL3000.A.H\_000623300), which is a non-essential gene encoding an excreted  
289 lysophospholipase in *T. brucei* (Monic et al., 2022, Tounkara et al., 2021). Repair cassettes  
290 containing either the phleomycin-resistant gene (*BleR*) flanked by 5' and 3' regulatory  
291 sequences or the marker-free *SBS* sequence were used to transfect BSF and PCF,  
292 respectively (**Figure 5A**). As above, the insertion of the repair cassettes was checked by  
293 PCR and sequencing from genomic DNA isolated from Phleomycin selection (*BleR* cassette)  
294 or cell cloning (*SBS* cassette). The four BSF clones tested are all homozygous mutants,  
295 further confirmed by western-blot analyses using an anti-*LysoPLA* immune serum showing  
296 that *LysoPLA* is no longer expressed (**Figure 5A/B/C**). Similarly, three out of the five PCF  
297 clones tested are homozygous mutants (**Figure 5D**, clones 1B6, 1E10 and 2C3), as  
298 confirmed by western-blot analyses (**Figure 5E**).

299 We also used *SpCas9* to inactivate the *GK* multigene family in *T. congolense*, which is  
300 composed of 3 *GK* copies per allele, one of which is a pseudogene with two frameshifts  
301 (**Figure 6A**, TcIL3000\_0\_55170, TriTrypDB). BSF were transfected with a *SpCas9*/gRNA  
302 complex and a repair *BleR* cassette containing 5' and 3' regulatory sequences. Among the  
303 four clones tested, three were homozygote mutants and one was heterozygote (**Figure**  
304 **6B**). The absence of *GK* expression was confirmed by western blot analyses using anti-*GK*  
305 antibodies (**Figure 6C**) and by quantitative proton NMR spectrometry analyses of excreted  
306 end products from the metabolism of [U- $^{13}\text{C}$ ]-glycerol and glucose (**Figure 6D**). Indeed,  
307 the production of  $^{13}\text{C}$ -enriched succinate and acetate from the metabolism of [U- $^{13}\text{C}$ ]-  
308 glycerol is abolished in a mutant cell line, while the conversion of non-enriched glucose to  
309 succinate and acetate is not affected (**Figure 6D**). In conclusion, our data clearly showed  
310 that transfection of RNP complexes containing *SpCas9* has the capacity to rapidly and  
311 efficiently modify all members of multigene families in *T. congolense* and probably all  
312 trypanosomatids.

313 **DISCUSSION**

314 Since 2014, kinetoplastid studies using CRISPR/Cas9 technology have all employed  
315 parasites that constitutively express Cas9, which required genome integration of the RNP-  
316 encoding gene, even gRNAs and in some cases. However, these potentially compromise  
317 parasite growth (Peng et al., 2014). More recently, Soares Medeiros *et al.* demonstrated  
318 that transfection of the Cas9-gRNA RNP complex also induced rapid and efficient genome  
319 editing in kinetoplastids, but only with a Cas9 derived from *Staphylococcus aureus*, and  
320 hypothesized that *SpCas9* was too large to be transfected and functional (Soares Medeiros  
321 *et al.*, 2017). In this current study, we demonstrate that *SpCas9* is fully functional and  
322 effective after transfection into the parasites. We have shown that both the commercial  
323 *SpCas9* (IDT) and the *SpCas9* produced in our laboratory enable rapid and efficient genome  
324 modification in several kinetoplastids (*T. brucei*, *T. congolense* and *Leishmania*), across  
325 different life cycle stages (insect and mammalian stages). We were able to target single  
326 genes and multigene families.

327 This approach based on transfection of RNP complexes offers several advantages including,  
328 (i) adaptability to any laboratory and field strains, (ii) for non-essential genes, both alleles  
329 are inactivated simultaneously, which is also valid for large multigene families, (iii) Cas9  
330 remains transiently in the transfected cell, preventing them from the deleterious effect of  
331 constitutive Cas9 expression, and (iv) no need for selection markers, which implies that  
332 numerous modifications can be achieved in the same cell line. Peng *et al.* demonstrated  
333 that mutations induced by Cas9 were mediated by MMEJ, a process that results in a  
334 deletion between homologous regions (Peng et al., 2014). We have also observed such  
335 deletions in *T. brucei* with both the commercial *SpCas9* (from IDT) and laboratory-  
336 produced *SpCas9*, in the absence of repair cassettes. This approach proved to be very  
337 efficient since we inactivated the *GFP* gene introduced in *T. brucei* PCF with an efficiency  
338 close to 50%, all within a few days. When double-strain breaks through Cas9 are combined  
339 with repair cassettes, it becomes easy to achieve targeted insertions through HDR, allowing  
340 inactivation or tagging of genes at their endogenous loci. We have thus been able to insert  
341 resistance markers (*BleR* and *PacR*), a gene encoding the RED fluorescent protein, or a  
342 short insertion sequence containing a series of stop codons enabling the inactivation of the  
343 target gene. We did not test the limit for the homology arms' size, but in *T. cruzi* and  
344 *Leishmania*, approximately 30 bp is sufficient (Soares Medeiros *et al.*, 2017). Finally, the  
345 insertion of short coding sequences at the 5' and/or 3' ends of the targeted genes (in order  
346 to tag them) can be achieved on both alleles without a selection marker and without  
347 significant modification of the UTRs (Morel *et al.*, 2023). In terms of efficiency, there  
348 appears to be no set rule, i.e., this may depend on the gRNA, the targeted gene, the stage  
349 of division, and how the parasites are selected. However, adding regulatory sequences  
350 upstream and downstream of the insertion cassette encoding a resistance marker, appears

351 to enhance the selection of homozygous clones for *T. brucei* BSF. We did not test the  
352 addition of regulatory sequences in *Leishmania* since the obtained homozygote rate was  
353 already very high (**Table 1**). In *T. cruzi*, successive transfections appear to significantly  
354 increase efficiency (Soares Medeiros et al., 2017), and this is an interesting approach when  
355 homozygous clones are not obtained. Here, we consistently obtained homozygous clones  
356 for non-essential genes. However, for genes suspected to be essential, only heterozygous  
357 clones are obtained. Therefore, successive transfections should enable the confirmation of  
358 their essentiality, if only heterozygous clones are obtained. It should be noted that  
359 successive transfections may also lead to the selection of chromosomal polysomy (Tovar  
360 et al., 1998).

361 Another important point to consider is the optimization of Cas9 for its importation by  
362 electroporation. Soares Medeiros et al. reported that recombinant *SpCas9* is not active on  
363 *T. cruzi*, which was interpreted as non-internalization by electroporation due to a size issue  
364 (Soares Medeiros et al., 2017). In agreement with their hypothesis, they showed the  
365 functionality of a smaller Cas9 (Cas9 from *Staphylococcus aureus*), which is abolished by  
366 fusion with GFP (Peng et al., 2014). However, the recombinant *SpCas9* is functional in the  
367 same experimental set up. The only difference between the recombinant *SpCas9* used by  
368 Soares Medeiros et al. and us is the presence of 2 and 3 NLS sequences, respectively.  
369 These data suggest that the size of the ribonucleoprotein complex is not a limiting factor,  
370 however the number of NLS sequences to achieve effective nuclear targeting seems to be  
371 an important factor to consider. Very recently, Minet et al. also managed to transfect and  
372 modify *T. congolense* bloodstream forms using a commercial *SpCas9*, which contains 3  
373 NLS in its sequence, further demonstrating that this protein is fully functional in  
374 kinetoplastids (Minet et al., 2023).

375 Finally, this system is likely functional in all cells that can be transfected, enabling more  
376 relevant studies on field strains. Indeed, this system is also valuable for studying cells that  
377 are difficult to cultivate (low cell density) and that previously required a significant number  
378 of cells for transfection through classical homologous recombination approaches. We used  
379  $5 \times 10^5$  cells to efficiently edit both alleles of the targeted genes, but we believe that this  
380 approach could be adapted to many fewer cells, provided that a sufficient number of clonal  
381 cells are sorted by flow cytometry. The transfection of the RNP-gRNA complex and its  
382 various derivatives, including dead Cas9, dCas9-methyltransferases, activators, etc.,  
383 presents a wealth of exciting research opportunities across diverse cell types (Engstler and  
384 Beneke, 2023, Gomaa et al., 2022). Notably, this innovative approach holds great promise  
385 for advancing our understanding of biological processes showing several redundant  
386 pathways, such as some metabolic capacities (Millerioux et al., 2018, Wargnies et al.,  
387 2018), for which the need to inactivate multiple enzymes has often been hampered by the  
388 scarcity of selection markers.

389 **EXPERIMENTAL PROCEDURES**

390 ***Trypanosomes and cell cultures***

391 The procyclic forms (PCF) of *T. brucei* EATRO1125.T7T (TetR-HYG-T7RNAPOL-NEO, where  
392 TetR stands for tetracycline resistance, HYG for hygromycin, T7RNAPOL for RNA  
393 polymerase T7, and NEO for neomycin) was cultured at 27°C with 5% CO<sub>2</sub> in SDM79  
394 medium containing 10% (vol/vol) heat-inactivated fetal calf serum, 5 µg/mL hemin, 0.04  
395 mg/mL streptomycin, 40 U/mL penicillin (SigmaP4333), 25 µg/mL hygromycin and 10  
396 µg/mL neomycin. The bloodstream forms (BSF) of *T. brucei* 427 90-13 (TetR-HYG-  
397 T7RNAPOL-NEO) was cultured at 37°C with 5% CO<sub>2</sub> in Iscove's modified Dulbecco's  
398 medium (IMDM) supplemented with 10% (vol/vol) heat-inactivated fetal calf serum, 0.2  
399 mM β-mercaptoethanol, 36 mM NaHCO<sub>3</sub>, 1 mM hypoxanthine, 0.16 mM thymidine, 1 mM  
400 sodium pyruvate, 0.05 mM bathocuproine, 1.5 mM L-cysteine, 5 µg/mL hygromycin and  
401 2.5 µg/mL neomycin. *L. infantum* 263 promastigote form was cultured at 27°C with 5%  
402 CO<sub>2</sub> in SDM79 medium containing 10% (vol/vol) heat-inactivated fetal calf serum, 5 µg/mL  
403 hemin, 0.04 mg/mL streptomycin and 40 U/mL penicillin (SigmaP4333). The BSF of *T.*  
404 *congolense* IL3000 was cultured at 34°C with 5% CO<sub>2</sub> in MEM medium (Sigma M0643)  
405 containing 20% (vol/vol) heat-inactivated goat serum (InvitroGen 16210072), 6 mg/mL  
406 HEPES, 2 mg/mL NaHCO<sub>3</sub>, 1 mg/mL glucose, 100 µg/mL sodium pyruvate, 10 µg/mL  
407 adenosine, 14 µg/mL hypoxanthine, 4 µg/mL thymidine, 14 µg/mL bathocuproine, 2 mM  
408 glutamine and 0.2 mM β-mercaptoethanol, pH 7.2 to 7.4. The PCF of *T. congolense* was  
409 cultured at 27°C with 5% CO<sub>2</sub> in MEM medium (Sigma M0643) containing 20% (vol/vol)  
410 heat-inactivated fetal calf serum, 6 mg/mL HEPES, 2 mg/mL NaHCO<sub>3</sub>, 5 µg/mL hemin, 2  
411 mM glutamine and 8 mM Proline, pH 7.3-7.4. Growth was monitored by daily cell counting  
412 with the cytometer Guava® Muse® or Guava® easyCyte™.

413

414 ***CRISPR/Cas9 inactivation***

415 Gene inactivation was achieved by inserting double-stranded DNA corresponding either to  
416 a resistance marker (phleomycin or puromycin), to a gene encoding a fluorescent protein  
417 (monomeric RED), or to a short sequence containing 6 successive stop codons in the 3  
418 reading phases and a *Bam*HI restriction site. These double-stranded DNA fragments were  
419 also flanked by 50 bp homologous to the 5' and 3' sequences of the Cas9 cut site. The  
420 EATRO1125.T7T PCF or 427 90.13 BSF (5x10<sup>5</sup> cells) were respectively transfected, using  
421 Amaxa nucleofectorII, with 1 µg of purified cassette (phleomycin or puromycin resistance  
422 marker, mRED or Stop*Bam*HIStop), 30 µg of Cas9 protein from IDT preloaded with a  
423 mixture of TracrRNA (0.4 µmol) and gRNA (0.4 µmol). Cells were transfected using  
424 program X-001 or U-033 for *T. congolense* and selected or not with phleomycin (for *T.*  
425 *brucei* PCF 5 µg/mL or BSF 2.5 µg/mL and for *T. congolense* PCF 2.5 µg/mL or BSF 5  
426 µg/mL) or puromycin (*T. brucei* PCF 1 µg/mL). Cells were cloned using a cell sorter (TBM

427 Core facility), and the selection of inactivated cells was performed by DNA extraction using  
428 the NucleoSpin Blood kit (Macherey-Nagel) followed by PCR amplification using primers  
429 flanking the Cas9 cleavage site, see supplemental **Table S2**. Guide RNA were designed  
430 using EuPaGDT (Peng and Tarleton, 2015), from <http://tritrypdb.org>. Primers and guide  
431 RNA used were synthesized by Integrated DNA Technologies (IDT) and listed in  
432 supplemental **Table S2**.

433

#### 434 ***Southern-blot***

435 A total of 2.5 µg of genomic DNA from *T. brucei* (EATRO1125.T7T) were subjected to *Kpn*I  
436 oe *Mfe*I digestion, electrophoresed in 0.8% agarose gel, blotted onto Hybond N<sup>+</sup> membrane  
437 (Amersham), and hybridized with labelled probe at 50°C in 6X SSPE (1X SSPE: 0.18 mM  
438 NaCl, 10 mM NaH<sub>2</sub>PO<sub>4</sub>, 1 mM ethylenediaminetetraacetate, pH 7.0), 0.1% SDS and  
439 washed at 50°C using 0.5X SSPE-0.1% SDS, before revelation. Probes were obtained by  
440 PCR using the primers pGK-S55 and pGK-S53 (**Table S1**) and labelled with the PCR DIG  
441 Probe Synthesis Kit (Roche) according to the manufacturer and revealed using the DIG  
442 Luminescent Detection Kit and DIG Easy Hyb (Roche).

443

#### 444 ***Western-blot***

445 Total protein extracts (5x10<sup>6</sup> cells) were separated by SDS-PAGE (10%) and  
446 immunoblotted on TransBlot Turbo Midi-size PVDF Membranes (Bio-Rad).  
447 Immunodetection was performed using the primary antibodies, diluted in PBS-Tween-Milk  
448 (0.05% Tween20, 5% skimmed milk powder), rabbit anti-GK (1:1,000), rabbit anti-  
449 LysoPLA (1:1,000) and mouse anti-enolase (1:100,000, gift from P.A.M. Michels,  
450 Edinburgh, UK). Revelation was performed using a second antibody coupled to the HRP  
451 (anti-rabbit or anti-mouse IgG conjugated to horseradish peroxidase, Bio-Rad, 1:5,000  
452 dilution) and detected using the Clarity Western enhanced-chemiluminescence (ECL)  
453 substrate as describes by the manufacturer (Bio-Rad). Images were acquired and analyzed  
454 with the ImageQuant Las 4000 luminescent image analyzer.

455

#### 456 ***Mitochondria staining on living cells***

457 Rhodamine-123 (30 µg/mL) was added to cell culture (5x10<sup>6</sup> - 1x10<sup>7</sup> cells per mL) for 15  
458 min at room temperature, then cells were washed twice with PBS and spread on slides.  
459 Images were acquired with MetaMorph software on Zeiss Axioplan 2 microscope and  
460 processed with ImageJ.

461

#### 462 ***Immunofluorescence***

463 Cells were washed twice with PBS, then fixed with 2% paraformaldehyde (PFA) for 10 min  
464 at room temperature and 0.1 mM glycine was added for 10 min to stop the reaction. The

465 cells were spread on slides and permeabilized with 0.05% triton X-100. After incubation in  
466 PBS containing 4% bovine serum albumin (BSA) for 20 min, cells were incubated for 1 h  
467 with primary antibodies diluted in PBS-BSA 4%, washed 4 times with PBS and incubated  
468 for 45 min with secondary antibodies diluted in PBS-BSA 4% followed by three washes.  
469 Kinetoplasts and nuclei were then labelled with DAPI (10 µg/mL) for 5 min. Slides were  
470 washed three times with PBS and mounted with SlowFade Gold (Molecular probes). Images  
471 were acquired with MetaMorph software on Zeiss Imager Z1 or Axioplan 2 microscope and  
472 processed with ImageJ.

473

474 ***Analysis of excreted end-products from the metabolism of carbon sources by***  
475 ***proton 1H-NMR.***

476 2 to 4x10<sup>7</sup> *T. brucei* PCF, *Leishmania* promastigote or *T. congolense* BSF cells were  
477 collected by centrifugation at 1,400 x g for 10 min, washed twice with phosphate-buffered  
478 saline supplemented with 2 g/L NaHCO<sub>3</sub> (pH 7.4) and incubated in 1 mL (single point  
479 analysis) of PBS supplemented with 2 g/L NaHCO<sub>3</sub> (pH 7.4). Cells were maintained for 6 h  
480 at 27°C in incubation buffer containing one <sup>13</sup>C-enriched carbon source (1 mM, [U-<sup>13</sup>C]-  
481 Glucose or [U-<sup>13</sup>C]-Glycerol or [U-<sup>13</sup>C]-Threonine; U stands for "uniformly <sup>13</sup>C-labelled"),  
482 except for *T. congolense* BSF, which were incubated for only 1h30 at 37°C. The integrity  
483 of the cells during the incubation was checked by microscopic observation. The supernatant  
484 (1 mL) was collected and 50 µL of maleate solution in Deuterated water (D<sub>2</sub>O; 10 mM) was  
485 added as an internal reference. <sup>1</sup>H-NMR spectra were performed at 500.19 MHz on a Bruker  
486 Avance III 500 HD spectrometer equipped with a 5 mm cryoprobe Prodigy. Measurements  
487 were recorded at 25°C. Acquisition conditions were as follows: 90° flip angle, 5,000 Hz  
488 spectral width, 32 K memory size, and 9.3 sec total recycle time. Measurements were  
489 performed with 64 scans for a total time close to 10 min 30 sec.

490

491 ***Cas9 cloning, expression and purification Cas9***

492 The eSpCas9(1.1) gene containing two nuclear localization signals (NLS) was obtained  
493 from Addgene (Plasmid #71814) and cloned into the pST32 vector, which contains two N-  
494 terminal and C-terminal His-tag (Gift from Fanny Boissier, INSERM U1212 CNRS 5320,  
495 University of Bordeaux), using the *Nco*I and *Eco*RI restriction sites. A third nuclear  
496 localization signals (SV40) was added by hybridization of two complementary primers  
497 (**Table S1**) containing the SV40 NLS and cloned in frame at the 3' end of the pST32-  
498 eSpCas9(1.1) vector using *Eco*RI and *Xho*I restriction sites, generating the vector pST32-  
499 eSpCas9(1.1)-3NLS (**Figure 1B**). The plasmid was then transformed into *E. coli* Rosetta  
500 2(DE3) competent cells (Novagen).

501 A bacterial preculture was grown overnight at 37°C with shaking and used to inoculate 100  
502 mL of LB-Miller medium (peptone 10 g, yeast-extract 5 g, NaCl 10 g, pH 7). The culture

503 was grown at 37°C with shaking to an optical density at 600 nm (OD600) of 0.6 to 0.8.  
504 Protein expression was induced by adding isopropyl- $\beta$ -D-thiogalactopyranoside (IPTG; 100  
505  $\mu$ M), and the culture was kept at 18°C with shaking overnight. Cells were harvested by  
506 centrifugation, and the pellet was resuspended in 10 mL lysis buffer containing 500 mM  
507 KCl, 20 mM Hepes, 5 mM imidazole, pH 7.5 and protease inhibitor cocktail without EDTA  
508 (Merck). After lysis by sonication (20 sec, 4 times), the soluble fraction was obtained by  
509 centrifugation (30,000  $\times$  g, 30 min at 4°C) and purified by immobilized metal ion affinity  
510 chromatography (IMAC) using a His-Select Nickel Affinity Gel (Sigma) in a fast protein  
511 liquid chromatography (FPLC) system (ÄKTA; GE Healthcare Life Sciences). All  
512 chromatographic steps were performed at 4°C. Two mL of His-Select Nickel resin were  
513 equilibrated in buffer and packed in a XK 10/50 mm column housing (Omnifit) with 20 mL  
514 lysis buffer. The cleared lysate was loaded on the column using a syringe at 1 mL/min rate.  
515 The column with bound protein was washed first with buffer (20 mM Hepes, 500 mM KCl,  
516 50 mM imidazole, pH 7.5) until the absorbance returned to baseline again. The protein was  
517 eluted by applying a gradient from 0% to 100% elution buffer (20 mM Hepes, 500 mM  
518 KCl, 1 M imidazole, pH 7.5) over 20 mL and collected in 2 mL fractions. All peak fractions  
519 were analyzed for the presence of eSpCas9(1.1)-3NLS using SDS-PAGE, and the purity  
520 was estimated to be ~80% based on band intensity (**Figure S1**). An alternative to the  
521 ÄKTA purification was to purified purify the Cas9 protein in batches using  $\text{Ni}^{2+}$ -resin and  
522 incubated for 30 min at 4°C. The resin was washed three times with 50 mM imidazole in  
523 500 mM NaCl, Tris-HCl pH 8 and 3 times with 250 mM imidazole in 500 mM NaCl, Tris-HCl  
524 pH 8. eSpCas9(1.1)-3NLS was eluted with 500 mM imidazole in 500 mM NaCl, Tris-HCl pH  
525 8. Fractions were analyzed by SDS-PAGE. The elution buffer was then exchanged for  
526 storage buffer (20 mM HEPES-KOH, 500 mM KCl, 1 mM DTT, pH 7.5) while concentrating  
527 the protein to a volume <1.5 mL using a 50,000 MWCO concentrator (Amicon) at 4,000  $\times$   
528 g. Buffer exchange prevented precipitation in the concentrator. The concentrated fraction  
529 was then centrifuged for 10 min at 16,900  $\times$  g at 4°C to remove all precipitated material.  
530 The protein concentration was determined using a bicinchoninic acid (BCA) protein assay  
531 kit (Thermo Scientific), and the yield was determined to be approximately 5 mg/100 mL  
532 of bacteria culture.  
533

### 534 **Statistical analysis**

535 Experiments were performed at least in triplicates. Statistical analyses were performed  
536 using Prism (GraphPad) software. The results are presented as mean  $\pm$  S.D. Where  
537 indicated the results were subjected to a two-sided student's t-test to determine statistical  
538 differences against the indicated group (Confidence interval 95% - P-value style:  
539 0.1234(ns); 0.0332 (\*); 0.0021 (\*\*); 0.0002 (\*\*\*); <0.0001 (\*\*\*\*)).  
540

541 **ACKNOWLEDGMENTS**

542 Cell sorter analyses were performed at the TBMCore facility (FACSility) on BD FACSaria™  
543 III Sorter and we thank Atika Zouine and Vincent Pitard for technical assistance, data  
544 acquisition and interpretation (TBMCore CNRS 3427, INSERM US005, Université de  
545 Bordeaux). We also thank the CRISP'edit platform for their valuable advice during the  
546 setup of the CRISPR system. We thank Keith Gull (University of Manchester) for providing  
547 us the anti-PFR antibody. The Bringaud and Robinson teams are supported by the Centre  
548 National de la Recherche Scientifique (CNRS, <https://www.cnrs.fr/>), the Université de  
549 Bordeaux (<https://www.u-bordeaux.fr/>) and the Agence Nationale de la Recherche (ANR,  
550 <https://anr.fr/>) through the ParaFrap "Laboratoire d'Excellence" (LabEx,  
551 <https://www.enseignementsup-recherche.gouv.fr/cid51355/laboratoires-d-excellence.html>) (ANR-11-LABX-0024). The Bringaud team is also supported by the  
552 "Fondation pour la Recherche Médicale" (FRM, <https://www frm.org/>) ("Equipe FRM", grant  
553 n°EQU201903007845) and the ANR grant ADIPOTRYP (ANR19-CE15-0004-01) and the  
554 Robinson team by the ANR grant Structu-Ring (ANR-20-CE91-0003). M.O is the holder of  
555 a Canada research Chair and the recipient of a CIHR Foundation Grant. He was the holder  
556 of a University de Bordeaux IDEX fellowship.  
557

558

559

560 **AUTHOR CONTRIBUTIONS**

561 AC, HP, MP, OQ, MCA, BM, MS performed experiments and contributed to analysis and  
562 interpretation of the data. PMV, BM, RDR, OM, RL, BF conceptualized the study, contributed  
563 to analysis and interpretation of the data, TE performed experiments, conceptualized the  
564 study, contributed to analysis and interpretation of the data and wrote the manuscript,  
565 with also an input from all the authors.

566 **REFERENCES**

567 ALLMANN, S., WARGNIES, M., PLAZOLLES, N., CAHOREAU, E., BIRAN, M., MORAND, P.,  
568 PINEDA, E., KULYK, H., ASENCIO, C., VILLAFRAZ, O., RIVIERE, L., TETAUD, E.,  
569 ROTUREAU, B., MOURIER, A., PORTAIS, J. C. & BRINGAUD, F. 2021. Glycerol  
570 suppresses glucose consumption in trypanosomes through metabolic contest. *PLoS*  
571 *Biol*, 19, e3001359.

572 BARRANGOU, R., FREMAUX, C., DEVEAU, H., RICHARDS, M., BOYAVAL, P., MOINEAU, S.,  
573 ROMERO, D. A. & HORVATH, P. 2007. CRISPR provides acquired resistance against  
574 viruses in prokaryotes. *Science*, 315, 1709-12.

575 BENEKE, T., MADDEN, R., MAKIN, L., VALLI, J., SUNTER, J. & GLUENZ, E. 2017. A CRISPR  
576 Cas9 high-throughput genome editing toolkit for kinetoplastids. *R Soc Open Sci*, 4,  
577 170095.

578 BOUTIN, J., ROSIER, J., CAPPELLEN, D., PRAT, F., TOUTAIN, J., PENNAMEN, P., BOURON,  
579 J., ROORYCK, C., MERLIO, J. P., LAMRISSI-GARCIA, I., CULLOT, G., AMINTAS, S.,  
580 GUYONNET-DUPERAT, V., GED, C., BLOUIN, J. M., RICHARD, E., DABERNAT, S.,  
581 MOREAU-GAUDRY, F. & BEDEL, A. 2021. CRISPR-Cas9 globin editing can induce  
582 megabase-scale copy-neutral losses of heterozygosity in hematopoietic cells. *Nat*  
583 *Commun*, 12, 4922.

584 BRINGAUD, F., BIRAN, M., MILLERIOUX, Y., WARGNIES, M., ALLMANN, S. & MAZET, M.  
585 2015. Combining reverse genetics and nuclear magnetic resonance-based  
586 metabolomics unravels trypanosome-specific metabolic pathways. *Mol Microbiol*,  
587 96, 917-26.

588 COUSTOU, V., PLAZOLLES, N., GUEGAN, F. & BALTZ, T. 2012. Sialidases play a key role  
589 in infection and anaemia in *Trypanosoma congolense* animal trypanosomiasis. *Cell*  
590 *Microbiol*, 14, 431-45.

591 CRAWFORD, E. D., QUAN, J., HORST, J. A., EBERT, D., WU, W. & DERISI, J. L. 2017.  
592 Plasmid-free CRISPR/Cas9 genome editing in *Plasmodium falciparum* confirms  
593 mutations conferring resistance to the dihydroisoquinolone clinical candidate SJ733.  
594 *PLoS One*, 12, e0178163.

595 D'ASTOLFO, D. S., PAGLIERO, R. J., PRAS, A., KARTHAUS, W. R., CLEVERS, H., PRASAD,  
596 V., LEBBINK, R. J., REHMANN, H. & GEIJSSEN, N. 2015. Efficient intracellular delivery  
597 of native proteins. *Cell*, 161, 674-690.

598 DESQUESNES, M., SAZMAND, A., GONZATTI, M., BOULANGE, A., BOSSARD, G.,  
599 THEVENON, S., GIMONNEAU, G., TRUC, P., HERDER, S., RAVEL, S., SERENO, D.,  
600 WALECKX, E., JAMONNEAU, V., JACQUIET, P., JITTAPALAPONG, S., BERTHIER, D.,  
601 SOLANO, P. & HEBERT, L. 2022. Diagnosis of animal trypanosomoses: proper use  
602 of current tools and future prospects. *Parasit Vectors*, 15, 235.

603 ENGSTLER, M. & BENEKE, T. 2023. Gene editing and scalable functional genomic screening  
604 in *Leishmania* species using the CRISPR/Cas9 cytosine base editor toolbox  
605 *LeishBASEedit*. *Elife*, 12.

606 FU, Y., FODEN, J. A., KHAYTER, C., MAEDER, M. L., REYON, D., JOUNG, J. K. & SANDER,  
607 J. D. 2013. High-frequency off-target mutagenesis induced by CRISPR-Cas  
608 nucleases in human cells. *Nat Biotechnol*, 31, 822-6.

609 GOMAA, F., LI, Z. H., BEAUDOIN, D. J., ALZAN, H., GIRGUIS, P. R., DOCAMPO, R. &  
610 EDGCOMB, V. P. 2022. CRISPR/Cas9-induced disruption of *Bodo saltans*  
611 paraflagellar rod-2 gene reveals its importance for cell survival. *Environ Microbiol*,  
612 24, 3051-3062.

613 INOUE, N., OTSU, K., FERRARO, D. M. & DONELSON, J. E. 2002. Tetracycline-regulated  
614 RNA interference in *Trypanosoma congoense*. *Mol Biochem Parasitol*, 120, 309-13.

615 ISHINO, Y., SHINAGAWA, H., MAKINO, K., AMEMURA, M. & NAKATA, A. 1987. Nucleotide  
616 sequence of the iap gene, responsible for alkaline phosphatase isozyme conversion  
617 in *Escherichia coli*, and identification of the gene product. *J Bacteriol*, 169, 5429-  
618 33.

619 JINEK, M., CHYLINSKI, K., FONFARA, I., HAUER, M., DOUDNA, J. A. & CHARPENTIER, E.  
620 2012. A programmable dual-RNA-guided DNA endonuclease in adaptive bacterial  
621 immunity. *Science*, 337, 816-21.

622 KIM, S., KIM, D., CHO, S. W., KIM, J. & KIM, J. S. 2014. Highly efficient RNA-guided  
623 genome editing in human cells via delivery of purified Cas9 ribonucleoproteins.  
624 *Genome Res*, 24, 1012-9.

625 KOLEV, N. G., TSCHUDI, C. & ULLU, E. 2011. RNA interference in protozoan parasites:  
626 achievements and challenges. *Eukaryot Cell*, 10, 1156-63.

627 KOVAROVA, J., NOVOTNA, M., FARIA, J., RICO, E., WALLACE, C., ZOLTNER, M., FIELD, M.  
628 C. & HORN, D. 2022. CRISPR/Cas9-based precision tagging of essential genes in  
629 bloodstream form African trypanosomes. *Mol Biochem Parasitol*, 249, 111476.

630 LANDER, N., CHIURILLO, M. A., STOREY, M., VERCESI, A. E. & DOCAMPO, R. 2016.  
631 CRISPR/Cas9-mediated endogenous C-terminal Tagging of *Trypanosoma cruzi*  
632 Genes Reveals the Acidocalcisome Localization of the Inositol 1,4,5-Trisphosphate  
633 Receptor. *J Biol Chem*, 291, 25505-25515.

634 LANDER, N., CHIURILLO, M. A., VERCESI, A. E. & DOCAMPO, R. 2017. Endogenous C-  
635 terminal Tagging by CRISPR/Cas9 in *Trypanosoma cruzi*. *Bio Protoc*, 7.

636 LANDER, N., LI, Z. H., NIYOGI, S. & DOCAMPO, R. 2015. CRISPR/Cas9-Induced Disruption  
637 of Paraflagellar Rod Protein 1 and 2 Genes in *Trypanosoma cruzi* Reveals Their Role  
638 in Flagellar Attachment. *MBio*, 6, e01012.

639 LIANG, X., POTTER, J., KUMAR, S., ZOU, Y., QUINTANILLA, R., SRIDHARAN, M., CARTE,  
640 J., CHEN, W., ROARK, N., RANGANATHAN, S., RAVINDER, N. & CHESNUT, J. D.

641 2015. Rapid and highly efficient mammalian cell engineering via Cas9 protein  
642 transfection. *J Biotechnol*, 208, 44-53.

643 MILLERIOUX, Y., MAZET, M., BOUYSSOU, G., ALLMANN, S., KIEMA, T. R., BERTIAUX, E.,  
644 FOUILLEN, L., THAPA, C., BIRAN, M., PLAZOLLES, N., DITTRICH-DOMERGUE, F.,  
645 CROUZOLS, A., WIERENGA, R. K., ROTUREAU, B., MOREAU, P. & BRINGAUD, F.  
646 2018. De novo biosynthesis of sterols and fatty acids in the *Trypanosoma brucei*  
647 procyclic form: Carbon source preferences and metabolic flux redistributions. *PLoS*  
648 *Pathog*, 14, e1007116.

649 MINET, C., CHANTAL, I. & BERTHIER, D. 2023. Recent advances in genome editing of  
650 bloodstream forms of *Trypanosoma congolense* using CRISPR-Cas9  
651 ribonucleoproteins: Proof of concept. *Exp Parasitol*, 252, 108589.

652 MOJICA, F. J., DIEZ-VILLASENOR, C., GARCIA-MARTINEZ, J. & SORIA, E. 2005.  
653 Intervening sequences of regularly spaced prokaryotic repeats derive from foreign  
654 genetic elements. *J Mol Evol*, 60, 174-82.

655 MONIC, S. G., LAMY, A., THONNUS, M., BIZARRA-REBELO, T., BRINGAUD, F., SMITH, T.  
656 K., FIGUEIREDO, L. M. & RIVIERE, L. 2022. A novel lipase with dual localisation in  
657 *Trypanosoma brucei*. *Sci Rep*, 12, 4766.

658 MOREL, C.A., ASENCIO, C., BLANCARD, C., SALIN, B., GONTIER, E., DUVEZIN-CAUBET,  
659 S., ROJO, M., BRINGAUD, F. & TETAUD, E. 2023. Identification of a novel and  
660 ancestral machinery involved in mitochondrial membrane branching in  
661 *Trypanosoma brucei*. *bioRxiv* doi: 10.1101/2023.06.28.546890

662 MOZDY, A. D., MCCAFFERY, J. M. & SHAW, J. M. 2000. Dnm1p GTPase-mediated  
663 mitochondrial fission is a multi-step process requiring the novel integral membrane  
664 component Fis1p. *J Cell Biol*, 151, 367-80.

665 NGO, H., TSCHUDI, C., GULL, K. & ULLU, E. 1998. Double-stranded RNA induces mRNA  
666 degradation in *Trypanosoma brucei*. *Proc Natl Acad Sci U S A*, 95, 14687-92.

667 PENG, D., KURUP, S. P., YAO, P. Y., MINNING, T. A. & TARLETON, R. L. 2014. CRISPR-  
668 Cas9-mediated single-gene and gene family disruption in *Trypanosoma cruzi*. *MBio*,  
669 6, e02097-14.

670 PENG, D. & TARLETON, R. 2015. EuPaGDT: a web tool tailored to design CRISPR guide  
671 RNAs for eukaryotic pathogens. *Microb Genom*, 1, e000033.

672 PINEDA, E., THONNUS, M., MAZET, M., MOURIER, A., CAHOREAU, E., KULYK, H., DUPUY,  
673 J. W., BIRAN, M., MASANTE, C., ALLMANN, S., RIVIERE, L., ROTUREAU, B.,  
674 PORTAIS, J. C. & BRINGAUD, F. 2018. Glycerol supports growth of the *Trypanosoma*  
675 *brucei* bloodstream forms in the absence of glucose: Analysis of metabolic  
676 adaptations on glycerol-rich conditions. *PLoS Pathog*, 14, e1007412.

677 REIS-CUNHA, J. L., VALDIVIA, H. O. & BARTHOLOMEU, D. C. 2018. Gene and Chromosomal  
678 Copy Number Variations as an Adaptive Mechanism Towards a Parasitic Lifestyle in  
679 Trypanosomatids. *Curr Genomics*, 19, 87-97.

680 RICO, E., JEACOCK, L., KOVAROVA, J. & HORN, D. 2018. Inducible high-efficiency CRISPR-  
681 Cas9-targeted gene editing and precision base editing in African trypanosomes. *Sci  
682 Rep*, 8, 7960.

683 RYAN, O. W., SKERKER, J. M., MAURER, M. J., LI, X., TSAI, J. C., PODDAR, S., LEE, M. E.,  
684 DELOACHE, W., DUEBER, J. E., ARKIN, A. P. & CATE, J. H. 2014. Selection of  
685 chromosomal DNA libraries using a multiplex CRISPR system. *Elife*, 3.

686 SHAW, S., KNUSEL, S., HOENNER, S. & RODITI, I. 2020. A transient CRISPR/Cas9  
687 expression system for genome editing in *Trypanosoma brucei*. *BMC Res Notes*, 13,  
688 268.

689 SLAYMAKER, I. M., GAO, L., ZETSCHE, B., SCOTT, D. A., YAN, W. X. & ZHANG, F. 2016.  
690 Rationally engineered Cas9 nucleases with improved specificity. *Science*, 351, 84-  
691 8.

692 SOARES MEDEIROS, L. C., SOUTH, L., PENG, D., BUSTAMANTE, J. M., WANG, W.,  
693 BUNKOFSKE, M., PERUMAL, N., SANCHEZ-VALDEZ, F. & TARLETON, R. L. 2017.  
694 Rapid, Selection-Free, High-Efficiency Genome Editing in Protozoan Parasites Using  
695 CRISPR-Cas9 Ribonucleoproteins. *MBio*, 8.

696 SOLLELIS, L., GHORBAL, M., MACPHERSON, C. R., MARTINS, R. M., KUK, N., CROBU, L.,  
697 BASTIEN, P., SCHERF, A., LOPEZ-RUBIO, J. J. & STERKERS, Y. 2015. First efficient  
698 CRISPR-Cas9-mediated genome editing in *Leishmania* parasites. *Cell Microbiol*, 17,  
699 1405-12.

700 TOUNKARA, M., BOULANGE, A., THONNUS, M., BRINGAUD, F., BELEM, A. M. G., BENGALY,  
701 Z., THEVENON, S., BERTHIER, D. & RIVIERE, L. 2021. Novel protein candidates for  
702 serodiagnosis of African animal trypanosomosis: Evaluation of the diagnostic  
703 potential of lysophospholipase and glycerol kinase from *Trypanosoma brucei*. *PLoS  
704 Negl Trop Dis*, 15, e0009985.

705 TOVAR, J., WILKINSON, S., MOTTRAM, J. C. & FAIRLAMB, A. H. 1998. Evidence that  
706 trypanothione reductase is an essential enzyme in *Leishmania* by targeted  
707 replacement of the tryA gene locus. *Mol Microbiol*, 29, 653-60.

708 WARGNIES, M., BERTIAUX, E., CAHOREAU, E., ZIEBART, N., CROUZOLS, A., MORAND, P.,  
709 BIRAN, M., ALLMANN, S., HUBERT, J., VILLAFRAZ, O., MILLERIOUX, Y., PLAZOLLES,  
710 N., ASENCIO, C., RIVIERE, L., ROTUREAU, B., BOSHART, M., PORTAIS, J. C. &  
711 BRINGAUD, F. 2018. Gluconeogenesis is essential for trypanosome development in  
712 the tsetse fly vector. *PLoS Pathog*, 14, e1007502.

713 ZHANG, W. W., LYPACZEWSKI, P. & MATLASHEWSKI, G. 2017. Optimized CRISPR-Cas9  
714 Genome Editing for *Leishmania* and Its Use To Target a Multigene Family, Induce

715 Chromosomal Translocation, and Study DNA Break Repair Mechanisms. *mSphere*,  
716 2.  
717 ZHANG, W. W. & MATLASZEWSKI, G. 2015. CRISPR-Cas9-Mediated Genome Editing in  
718 *Leishmania donovani*. *mBio*, 6, e00861.  
719  
720

721

**Table 1 - Summary of the various CRISPR/Cas9 inactivation experiments.**

Gene targeted	Parasite	Inactivation cassette	Numbers of tested clones	Homozygous	Heterozygous	Both alleles inactivated (%)
<b>Fis1</b>	<i>T. brucei</i> PCF	<i>BleR + 3'/5' UTR</i>	5	5	0	100
	<i>T. brucei</i> BSF		12	1	11	8
	<i>T. brucei</i> BSF	<i>PacR</i> without UTR	34	0	33	0
	<i>T. brucei</i> BSF	SBS	76	2	3	3
<b>GK</b>	<i>T. brucei</i> PCF	<i>BleR + 3'/5' UTR</i>	11	11	0	100
<b>ALDH</b>	<i>L. infantum</i> Pro	<i>PacR</i> without UTR	39	12	1	31
	<i>L. infantum</i> Pro	<i>mRED</i> without UTR	6	5	1	83
	<i>L. infantum</i> Pro	SBS	12	4	0	33
<b>LysoPLA</b>	<i>T. congolense</i> BSF	<i>BleR + 3'/5' UTR</i>	4	4	0	100
	<i>T. congolense</i> PCF	SBS	5	3	0	60
<b>GK</b>	<i>T. congolense</i> BSF	<i>BleR + 3'/5' UTR</i>	4	3	1	75

722

SBS: short sequence containing a succession of stop codons

739 **Figure legends**

740

741 **Figure 1 - GFP inactivation in *T. brucei* PCF. (A)** Fluorescence flow cytometry analysis  
742 of *T. brucei* constitutively expressing a cytosolic GFP. GFP fluorescence was monitored over  
743 time from 24 to 72 h after transfection with 20 µg (no Cas9, Cas9/gRNA GFP1, Cas9/gRNA  
744 GFP2, Cas9/gRNA GFP3) or 60 µg (Cas9/gRNA GFP2) of RNP complexes from IDT, and a  
745 bar chart showing the percentage of GFP-negative cells at 72 to 144 h after transfection  
746 with the different guides. **(B)** The top panel shows a schematic representation of the  
747 plasmid allowing eSpCas9 expression in *E. coli*. The blue boxes represent the two  
748 polyhistidine sequences at the N and C-termini of the protein, the red boxes represent the 3  
749 nuclear localization signals (NLS), the black box represents 3 repeats of the FLAG epitope  
750 and the orange box represents the eSpCas9 coding sequence. The bottom panel shows the  
751 fluorescence flow cytometry analysis of *T. brucei* expressing the GFP monitored at 72 h  
752 after transfection with RNPs complexes from IDT or laboratory-purified (Lab) (no Cas9, 20  
753 µg Cas9/gRNA GFP2, 40 µg Cas9/gRNA GFP2, 40, 60 and 80 µg Cas9/gRNA GFP2). **(C)**  
754 Sequence comparison of a portion of the GFP gene from clones no longer expressing GFP.  
755 The sequence shows only the region targeted by the GFP2 guide RNA. The gray boxes (H1  
756 and H2) highlight the homology regions probably used for repair by MMEJ. Sequences  
757 resulting from inactivation by laboratory-purified Cas9 and those from commercial Cas9  
758 are labeled Lab and IDT respectively. Below is shown the corresponding chromatogram of  
759 the Dc6 and Ba10 clones.

760

761

762 **Figure 2 - Inactivation of the *TbFis1* gene in both *T. brucei* PCF and BSF. (A)**  
763 Schematic representation of the *TbFis1* locus and the two inactivation strategies by  
764 inserting the phleomycin resistance marker (*BleR*) or a short sequence containing a  
765 succession of stop codons (*SBS*). The position of the guide RNA is indicated by a vertical  
766 arrow (*TbFis1\_248*) and the 50-bp flanking sequences allowing repair through HDR are  
767 shown in gray. **(B)** PCR confirmation of *TbFis1* gene inactivation on both alleles in PCF and  
768 BSF cells. PCR products (primer ET24/ET25) are directly analyzed on agarose gel (*Fis1<sup>-/-</sup>*  
769 *BleR*) or after its digestion with *Bam*HI (*Fis1<sup>-/-</sup> SBS*), allowing easy discrimination of gene  
770 inactivation on both alleles. **(C)** Chromatogram of the *TbFis1* sequence highlighting the  
771 insertion of the *SBS* cassette.

772

773

774 **Figure 3 - Inactivation of the multigenic family encoding the glycerol kinase (GK)**  
775 **in *T. brucei* PCF. (A)** Schematic representation of the two alleles of the *GK* family in *T.*  
776 *brucei* and the inactivation strategy used by insertion of the phleomycin resistance marker  
*BleR*. The position of the guide RNA is indicated by a vertical arrow (*GK\_325rc*) and the

777 50-bp flanking sequences allowing repair through HDR are shown in gray. The position of  
778 the probe used for the Southern-blot analysis is indicated by a black box. **(B)** Confirmation  
779 by PCR of *GK* gene inactivation on both alleles in PCF. PCR products from various  
780 phleomycin-resistant clones (primer pGK-crispr-ctl5'/pGK-crispr-ctl3') are analyzed on an  
781 agarose gel. **(C)** Southern-blot analysis of various phleomycin-resistant clones. The two  
782 bands detected in the parental cells (WT) correspond to the *GK* copy located at the 5'  
783 extremity of the clusters (one asterisk) and to all the other *GK* copies (two asterisks). The  
784 insertion of the resistance marker increases the size of both of these bands by 880 bp in  
785 the phleomycin-resistant clones. **(D)** Western blot analysis of whole-cell extracts from  
786 different phleomycin-resistant *T. brucei* PCF clones. RNAi targeting *GK* was included as a  
787 control (Pineda et al., 2018). Antibodies against the paraflagellar rod (PFR) were used as  
788 a loading control. **(E)** <sup>1</sup>H-NMR analysis of <sup>13</sup>C-enriched end products (succinate and  
789 acetate, <sup>13</sup>C-Suc and <sup>13</sup>C-Ace, respectively) excreted from the metabolism of [U-<sup>13</sup>C]-  
790 glucose and [U-<sup>13</sup>C]-glycerol, by the parental (WT) and clone 2E6 (*GK*<sup>-/-</sup>) PCF cells. A  
791 portion of each spectrum ranging from 1.6 ppm to 2.6 ppm is presented.

792

793 **Figure 4 - ALDH inactivation in *L. infantum* promastigote. (A)** Schematic  
794 representation of the *ALDH* locus and the three inactivation strategies used, *i.e.*, insertion  
795 of the puromycin resistance marker (*PacR*), of the monomeric RED fluorescent protein  
796 (*mRED*) or of a short sequence containing a succession of stop codons (*SBS*). The position  
797 of the guide RNA is indicated by a vertical arrow (ALDH\_864) and the 50-bp flanking  
798 sequences allowing repair through HDR are shown in gray. **(B)** Confirmation by PCR of  
799 *ALDH* gene inactivation on both alleles. PCR products from phleomycin-resistant, RED  
800 fluorescent and *SBS* clones (primer ET62/ET63) are analyzed on an agarose gel. In the  
801 case of the *SBS* strategy, the PCR product was digested by *BamHI*. **(C)** The chimeric  
802 *ALDH/mRED* protein is expressed in the mitochondrion. The subcellular localization of  
803 *ALDH/mRED* in the *ALDH*<sup>-/-</sup> D3 clone (c1) was revealed by *mRED* fluorescence and  
804 compared to the cytosolic expression of *mRED* (c2). **(D)** Portion of the chromatogram  
805 showing the fusion of the *mRED* sequence with the *ALDH* sequence. **(E)** <sup>1</sup>H-NMR analysis  
806 of <sup>13</sup>C-enriched end products (<sup>13</sup>C-acetate, <sup>13</sup>C-Ace) excreted from metabolism of [U-<sup>13</sup>C]-  
807 threonine metabolism by the parental (WT), *ALDH*<sup>-/-</sup> *PacR* clone 1B1 re-expressing (*ALDH*<sup>-/-</sup>  
808 *PacR* +*ALDH*) or not the *ALDH* genes and *ALDH*<sup>-/-</sup> *SBS* clone A1 re-expressing (*ALDH*<sup>-/-</sup>  
809 *PacR* +*ALDH*) or not the *ALDH* gene. A rescue control was performed by expressing GFP in  
810 the *ALDH*<sup>-/-</sup> *PacR* clone. A portion of each spectrum ranging from 1.65 ppm to 2.05 ppm is  
811 presented.

812

813 **Figure 5 - Inactivation of the *LysoPLA* in *T. congolense* BSF and PCF. (A)** Schematic  
814 representation of the *LysoPLA* locus in *T. congolense* and the two inactivation strategies

815 used, *i.e.*, insertion of the phleomycin resistance marker (*BleR*) or a short sequence  
816 containing a succession of stop codons (*SBS*). The position of the guide RNA is indicated  
817 by a vertical arrow (*TcPLA\_370*) and the 50-bp flanking sequences allowing repair through  
818 HDR are shown in gray. **(B)** Confirmation of *LyoPLA* gene inactivation on both alleles in  
819 *T. congolense* BSF cells, by PCR analysis of various phleomycin-resistant clones (primer  
820 ET261/ET262). **(C)** Western blot analysis of whole-cell extracts from two phleomycin-  
821 resistant *T. congolense* BSF clones. Antibodies against enolase were used as a loading  
822 control. **(D)** Confirmation of *LyoPLA* gene inactivation on both alleles in *T. congolense*  
823 PCF cells by agarose gel analysis of *Bam*HI-digested PCR products from various  
824 phleomycin-resistant clones (primer ET261/ET262). The "Mix cells" lane corresponds to  
825 the cell population before cloning, containing parental cells, and heterozygous and  
826 homozygous mutants. The asterisk indicates the 456-bp band, which does not contain a  
827 *Bam*HI restriction site. Clones 2D5 and 1E11 exhibit the wild-type profile. **(E)** Western blot  
828 analysis of whole-cell extracts from marker-free (*SBS*) *T. congolense* PCF clones.  
829 Antibodies against enolase were used as a loading control.

830

831 **Figure 6 - Inactivation of the multigenic family encoding the glycerol kinase (GK)**  
832 **in *T. congolense* BSF. (A)** Schematic representation of the *GK* locus and its inactivation  
833 by inserting the phleomycin resistance marker *BleR*. The position of the guide RNA is  
834 indicated by a vertical arrow (*TcGK\_1097*) and the 50-bp flanking sequences allowing  
835 repair through HDR are shown in gray. **(B)** PCR confirmation of *GK* gene inactivation on  
836 both alleles in two different BSF clones. **(C)** Western blot analysis of whole-cell extracts  
837 from two phleomycin-resistant *T. congolense* BSF clones. **(D)** <sup>1</sup>H-NMR analysis of end  
838 products (succinate and acetate) excreted from the metabolism of glucose and [U-<sup>13</sup>C]-  
839 glycerol by the parental (WT) and clone C6 (GK<sup>-/-</sup>) BSF cell lines. A portion of each spectrum  
840 ranging from 1.3 ppm to 2.7 ppm is presented. In the NMR experiments, *T. congolense*  
841 BSF were incubated in the presence of a mixture of D-glucose (1 mM) and D-[U-<sup>13</sup>C]-  
842 glycerol (5 mM) to keep them alive. Resonances were assigned as follows: Ace, acetate;  
843 <sup>13</sup>C-Ace, <sup>13</sup>C-enriched acetate; Suc, succinate; <sup>13</sup>C-Suc, <sup>13</sup>C-enriched succinate; Pyr,  
844 pyruvate.

845

846 **Figure S1 - Expression and purification of the eSpCas9 from *E. coli*.** The eSpCas9  
847 protein expressed in *E. coli* was purified on a His-Select Nickel column. P, pellet; S,  
848 supernatant; Unbound, protein not retained on the column; Wash1 and 2 correspond to  
849 the wash fractions; E1 to E3 correspond to the elution fractions. The last lane represents  
850 5 µg of purified Cas9 commercially available from IDT.

851

852 **Figure S2 - Inactivation of the *TbFis1* gene in both *T. brucei* PCF and BSF.**  
853 Mitochondrial structure analysis using rhodamine 123 staining on living parental (WT) and  
854 *TbFis1*<sup>-/-</sup> PCF cell lines, and with immunofluorescence using an antibody directed against  
855 Hsp60 to label and visualize mitochondrial shape in BSF cells. Only the BSF were labeled  
856 with DAPI.

857

858 **Figure S3 - Inactivation of the multigenic family encoding the glycerol kinase**  
859 **(GK) in *T. brucei* PCF. (A)** Schematic representation of the two alleles of the *GK* gene  
860 cluster in *T. brucei*. The position of the probe used for the Southern-blot analysis is  
861 indicated by a black box. **(B)** Southern blot analysis of various phleomycin-resistant  
862 clones. Genomic DNA was digested with *Mfe*I, separated on a 0.8% agarose gel,  
863 transferred to a membrane (Hybond-N), and probed with a PCR product labeled with the  
864 PCR DIG Probe Synthesis Kit (Roche). The two bands detected in the parental cell line (WT)  
865 correspond to the allele containing 5 (one asterisk) or 6 (two asterisk) copies of the *GK*  
866 gene. The insertion of the resistance marker into the various copies of *GK* can either  
867 increase the size of the *Mfe*I fragment or reduce it if deletion of *GK* copies occurred by  
868 homologous recombination after Cas9 cleavage.

869

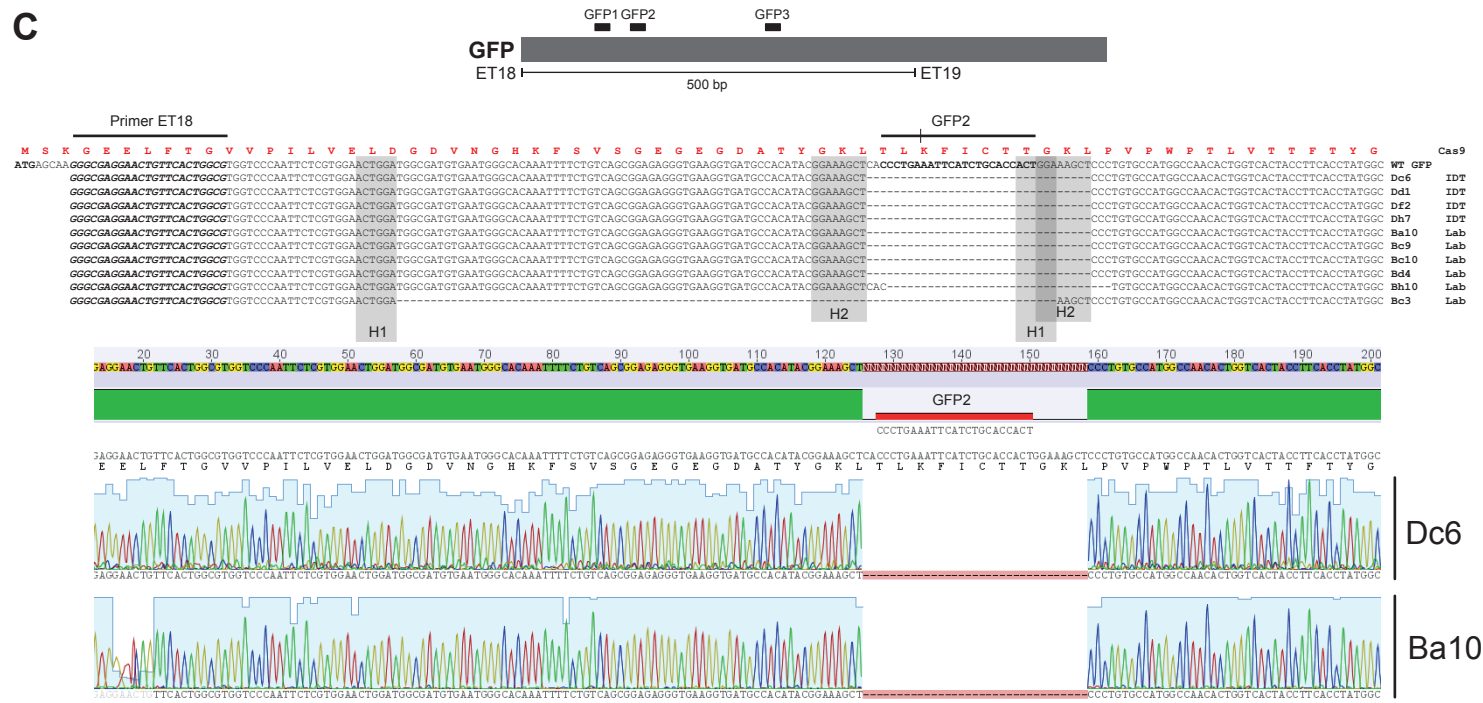
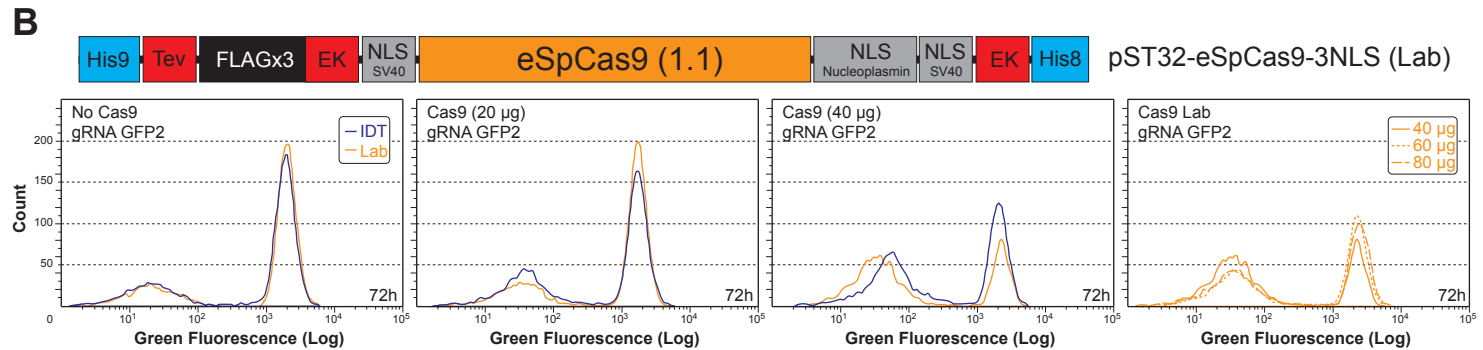
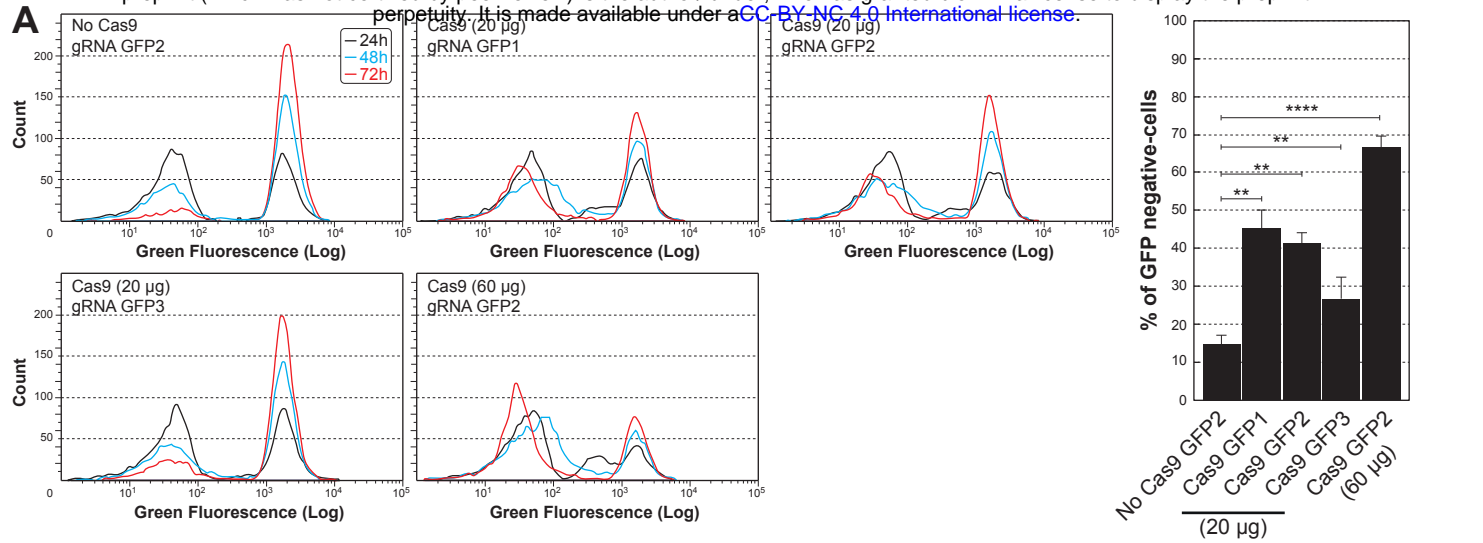


**Figure 1 - GFP inactivation in *T. brucei* PCF. (A)** Fluorescence flow cytometry analysis of *T. brucei* constitutively expressing a cytosolic GFP. GFP fluorescence was monitored over time from 24 to 72 h after transfection with 20 µg (no Cas9, Cas9/gRNA GFP1, Cas9/gRNA GFP2, Cas9/gRNA GFP3) or 60 µg (Cas9/gRNA GFP2) of RNP complexes from IDT, and a bar chart showing the percentage of GFP-negative cells at 72 to 144 h after transfection with the different guides. **(B)** The top panel shows a schematic representation of the plasmid allowing eSpCas9 expression in *E. coli*. The blue boxes represent the two polyhistidine sequences at the N and C-termini of the protein, the red boxes represent the cleavage sites of TEV and enterokinase (EK) proteases, the gray boxes represent the 3 nuclear localization signals (NLS), the black box represents 3 repeats of the FLAG epitope and the orange box represents the eSpCas9 coding sequence. The bottom panel shows the fluorescence flow cytometry analysis of *T. brucei* expressing the GFP monitored at 72 h after transfection with RNPs complexes from IDT or laboratory-purified (Lab) (no Cas9, 20 µg Cas9/gRNA GFP2, 40 µg Cas9/gRNA GFP2, 40, 60 and 80 µg Cas9/gRNA GFP2). **(C)** Sequence comparison of a portion of the GFP gene from clones no longer expressing GFP. The sequence shows only the region targeted by the GFP2 guide RNA. The gray boxes (H1 and H2) highlight the homology regions probably used for repair by MMEJ. Sequences resulting from inactivation by laboratory-purified Cas9 and those from commercial Cas9 are labeled Lab and IDT respectively. Below is shown the corresponding chromatogram of the Dc6 and Ba10 clones.

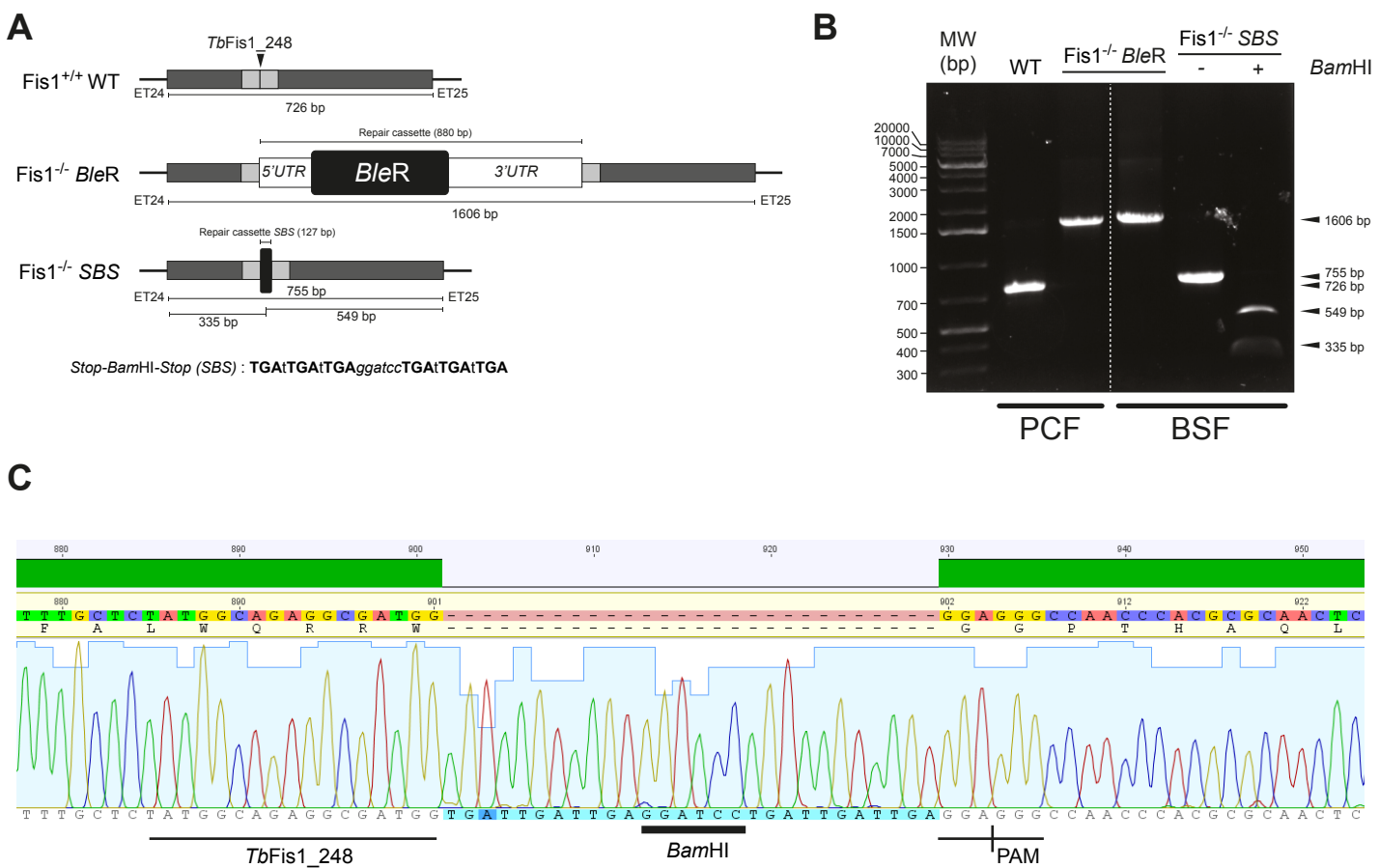
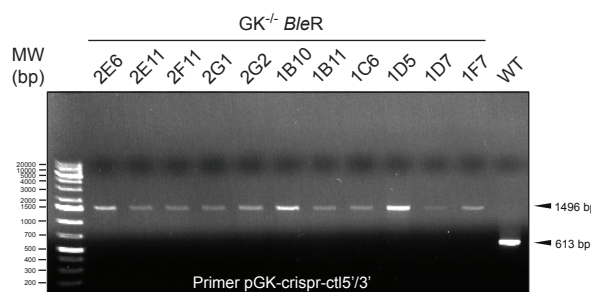
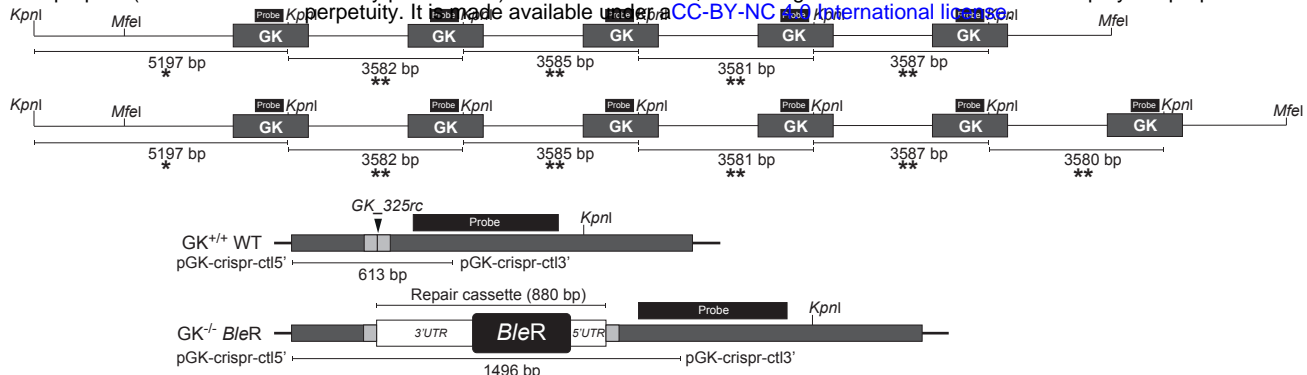
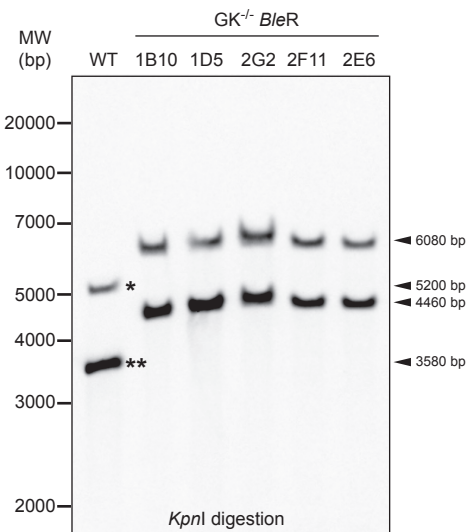


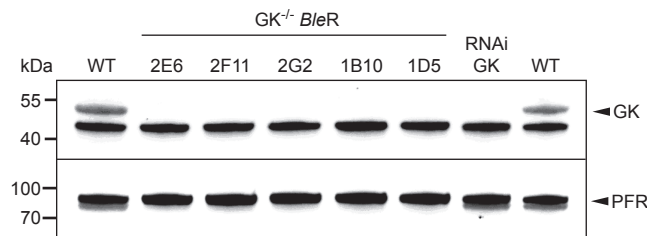
**Figure 2 - Inactivation of the *TbFis1* gene in both *T. brucei* PCF and BSF. (A)** Schematic representation of the *TbFis1* locus and the two inactivation strategies by inserting the phleomycin resistance marker (*BleR*) or a short sequence containing a succession of stop codons (*SBS*). The position of the guide RNA is indicated by a vertical arrow (*TbFis1\_248*) and the 50-bp flanking sequences allowing repair through HDR are shown in gray. **(B)** PCR confirmation of *TbFis1* gene inactivation on both alleles in PCF and BSF cells. PCR products (primer ET24/ET25) are directly analyzed on agarose gel (*Fis1<sup>-/-</sup> BleR*) or after its digestion with *BamHI* (*Fis1<sup>-/-</sup> SBS*), allowing easy discrimination of gene inactivation on both alleles. **(C)** Chromatogram of the *TbFis1* sequence highlighting the insertion of the *SBS* cassette.



**C**



**D**



**E**

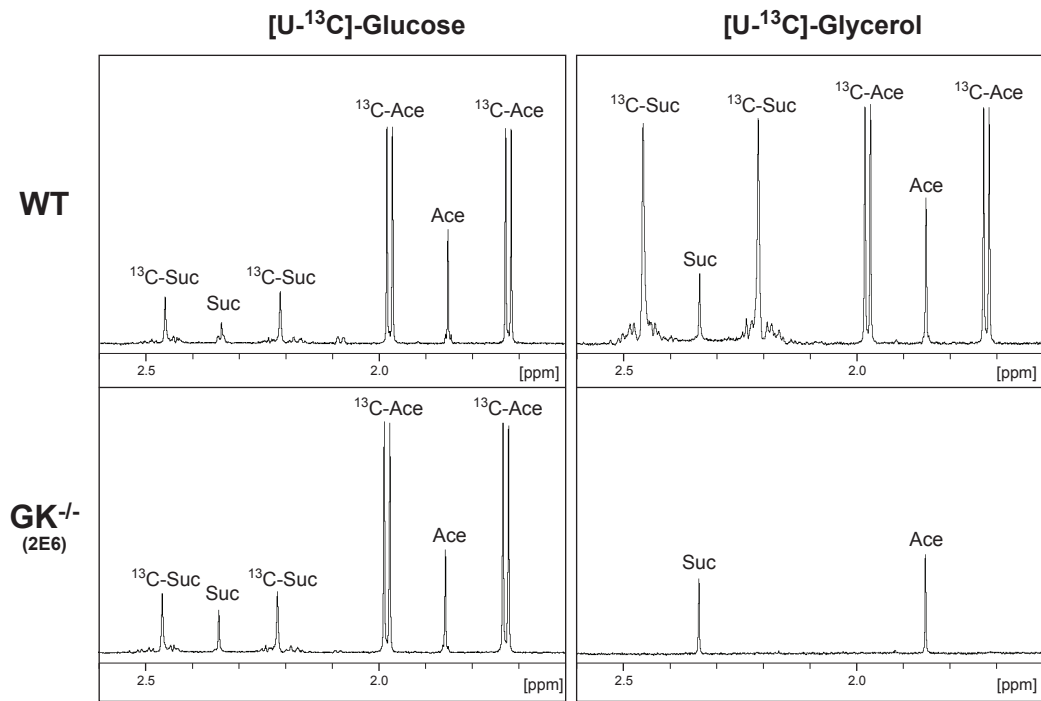
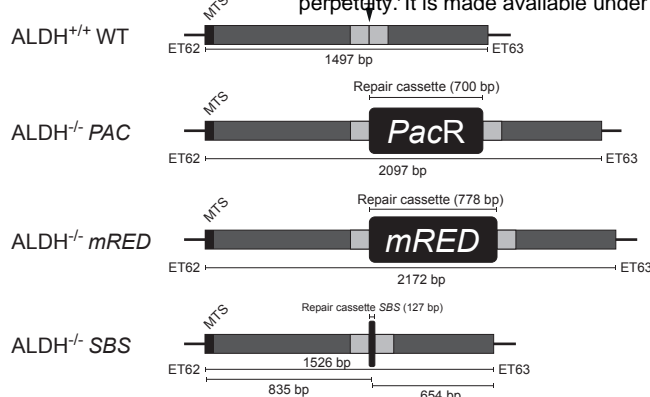


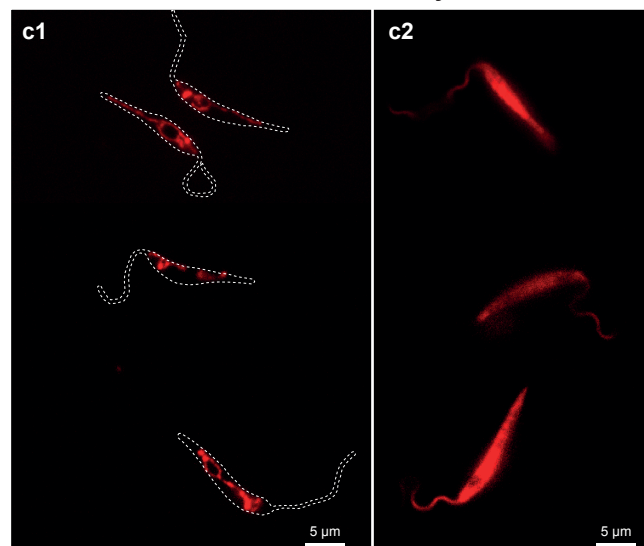
**Figure 3 - Inactivation of the multigenic family encoding the glycerol kinase (GK) in *T. brucei* PCF.** (A) Schematic representation of the two alleles of the GK family in *T. brucei* and the inactivation strategy used by insertion of the phleomycin resistance marker *BleR*. The position of the guide RNA is indicated by a vertical arrow (GK\_325rc) and the 50-bp flanking sequences allowing repair through HDR are shown in gray. The position of the probe used for the Southern-blot analysis is indicated by a black box. (B) Confirmation by PCR of GK gene inactivation on both alleles in PCF. PCR products from various phleomycin-resistant clones (primer pGK-crispr-ctl5'/pGK-crispr-ctl3') are analyzed on an agarose gel. (C) Southern-blot analysis of various phleomycin-resistant clones. The two bands detected in the parental cells (WT) correspond to the GK copy located at the 5' extremity of the clusters (one asterisk) and to all the other GK copies (two asterisks). The insertion of the resistance marker increases the size of both of these bands by 880 bp in the phleomycin-resistant clones. (D) Western blot analysis of whole-cell extracts from different phleomycin-resistant *T. brucei* PCF clones. RNAi targeting GK was included as a control (Pineda et al., 2018). Antibodies against the paraflagellar rod (PFR) were used as a loading control. (E) <sup>1</sup>H-NMR analysis of <sup>13</sup>C-enriched end products (succinate and acetate, <sup>13</sup>C-Suc and <sup>13</sup>C-Ace, respectively) excreted from the metabolism of [U-<sup>13</sup>C]-glucose and [U-<sup>13</sup>C]-glycerol, by the parental (WT) and clone 2E6 (GK<sup>-/-</sup>) PCF cells. A portion of each spectrum ranging from 1.6 ppm to 2.6 ppm is presented.

**A**

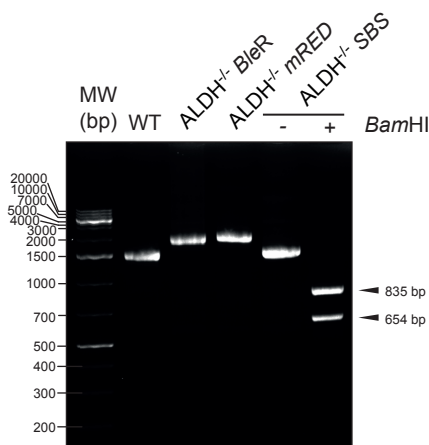


**C**

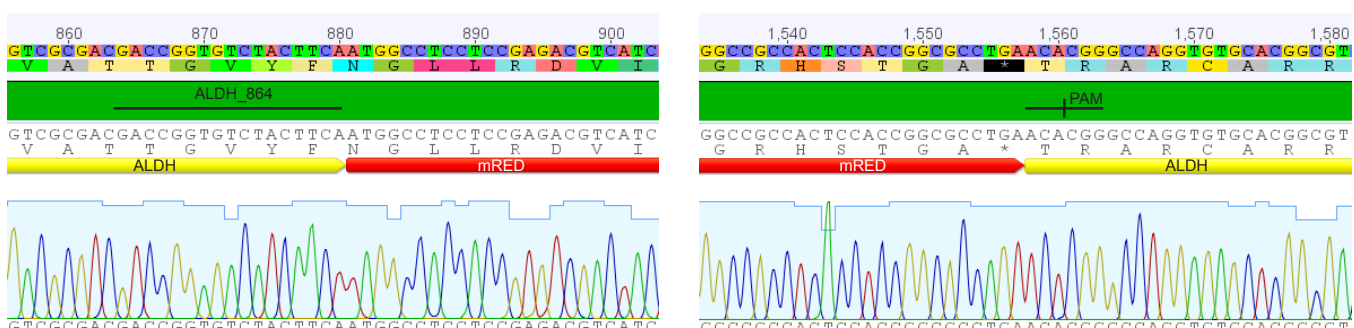
ALDH-/- *mRED* clone D3 Cytosolic *mRED*



**B**

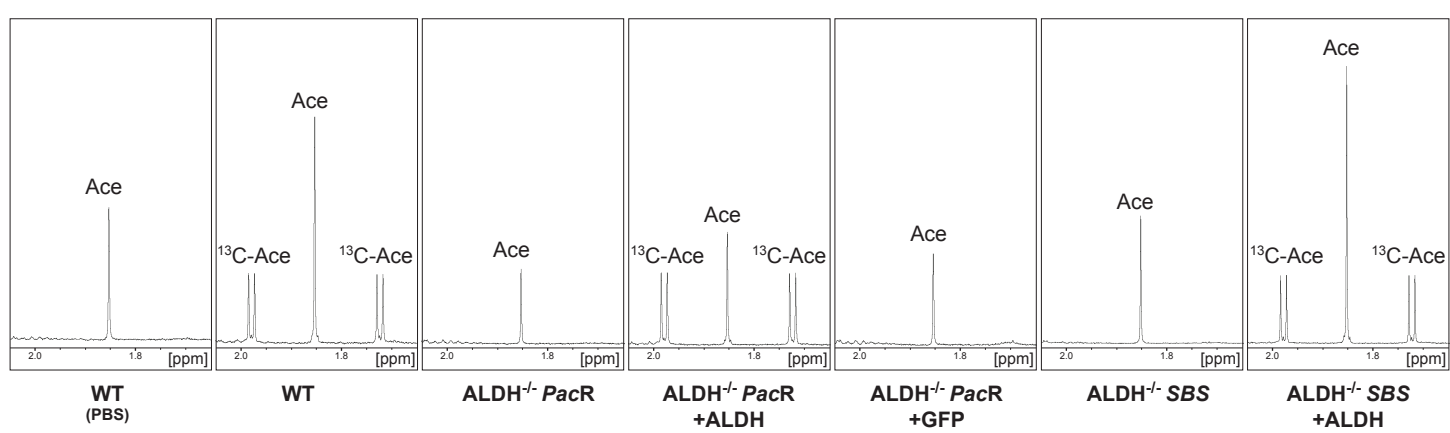


**D**



**E**

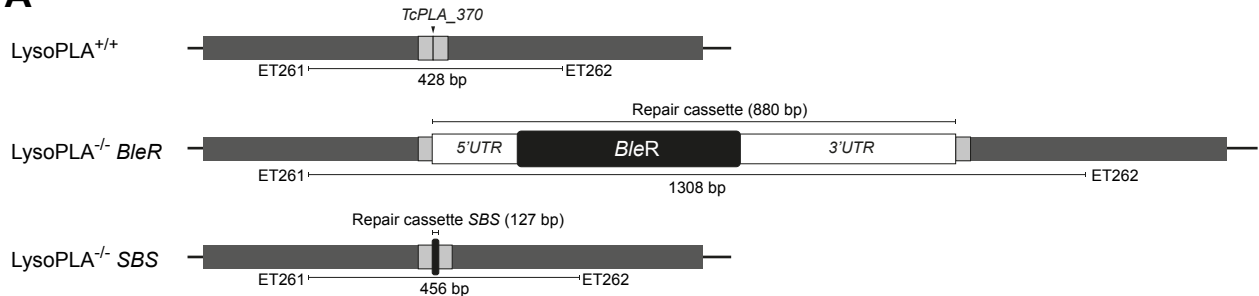
Threonine → Acetaldehyde → Acetate



[U-<sup>13</sup>C]-Threonine

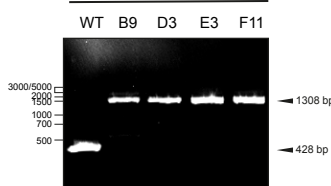
**Figure 4 - ALDH inactivation in *L. infantum* promastigote.** (A) Schematic representation of the ALDH locus and the three inactivation strategies used i.e., insertion of the puromycin resistance marker (*PacR*), of the monomeric RED fluorescent protein (*mRED*) or of a short sequence containing a succession of stop codons (*SBS*). The position of the guide RNA is indicated by a vertical arrow (ALDH\_864) and the 50-bp flanking sequences allowing repair through HDR are shown in gray. (B) Confirmation by PCR of ALDH gene inactivation on both alleles. PCR products from phleomycin-resistant, RED fluorescent and SBS clones (primer ET62/ET63) are analyzed on an agarose gel. In the case of the SBS strategy, the PCR product was digested by *BamHI*. (C) The chimeric ALDH/mRED protein is expressed in the mitochondrion. The subcellular localization of ALDH/mRED in the ALDH-/- D3 clone (c1) was revealed by mRED fluorescence and compared to the cytosolic expression of mRED (c2). (D) Portion of the chromatogram showing the fusion of the mRED sequence with the ALDH sequence. (E) <sup>1</sup>H-NMR analysis of <sup>13</sup>C-enriched end products (<sup>13</sup>C-acetate, <sup>13</sup>C-Ace) excreted from metabolism of [U-<sup>13</sup>C]-threonine metabolism by the parental (WT), ALDH-/- *PacR* clone 1B1 re-expressing (ALDH-/- *PacR* +ALDH) or not the ALDH genes and ALDH-/- SBS clone A1 re-expressing (ALDH-/- *PacR* +ALDH) or not the ALDH gene. A rescue control was performed by expressing GFP in the ALDH-/- *PacR* clone. A portion of each spectrum ranging from 1.65 ppm to 2.05 ppm is presented.

**A**



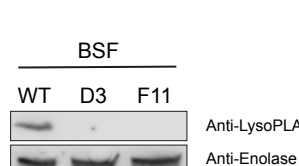
**B**

BSF



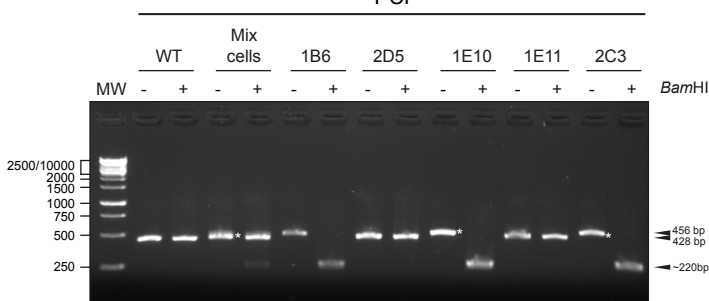
**C**

BSF



**D**

PCF



**E**

PCF

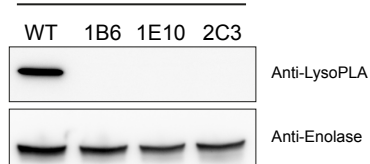
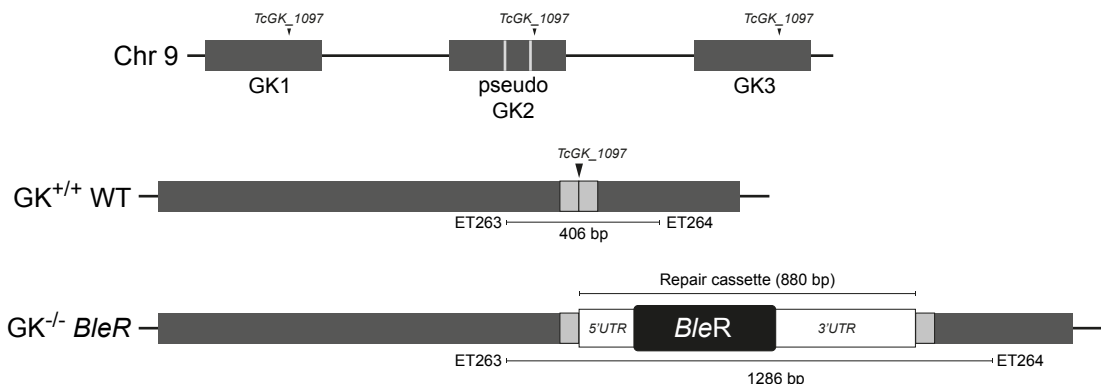
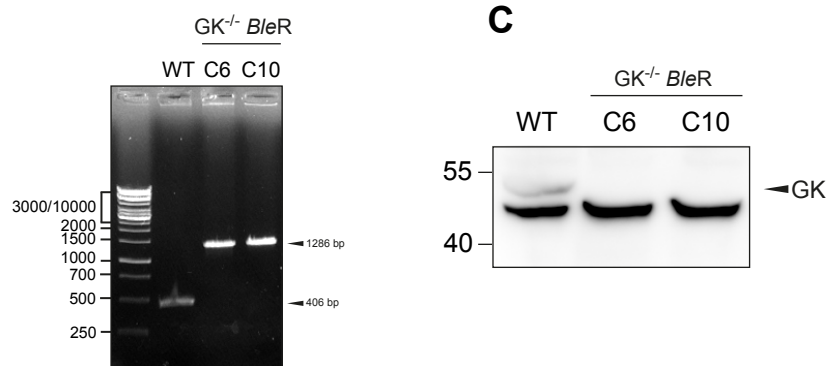


**Figure 5 - Inactivation of the LysoPLA in *T. congolense* BSF and PCF.** (A) Schematic representation of the LysoPLA locus in *T. congolense* and the two inactivation strategies used i.e., insertion of the phleomycin resistance marker (*BleR*) or a short sequence containing a succession of stop codons (SBS). The position of the guide RNA is indicated by a vertical arrow (*TcPLA\_370*) and the 50-bp flanking sequences allowing repair through HDR are shown in gray. (B) Confirmation of LysoPLA gene inactivation on both alleles in *T. congolense* BSF cells, by PCR analysis of various phleomycin-resistant clones (primer ET261/ET262). (C) Western blot analysis of whole-cell extracts from two phleomycin-resistant *T. congolense* BSF clones. Antibodies against enolase were used as a loading control. (D) Confirmation of LysoPLA gene inactivation on both alleles in *T. congolense* PCF cells by agarose gel analysis of *BamHI*-digested PCR products from various phleomycin-resistant clones (primer ET261/ET262). The "Mix cells" lane corresponds to the cell population before cloning, containing parental cells, and heterozygous and homozygous mutants. The asterisk indicates the 456-bp band, which does not contain a *BamHI* restriction site. Clones 2D5 and 1E11 exhibit the wild-type profile. (E) Western blot analysis of whole-cell extracts from marker-free (SBS) *T. congolense* PCF clones. Antibodies against enolase were used as a loading control.

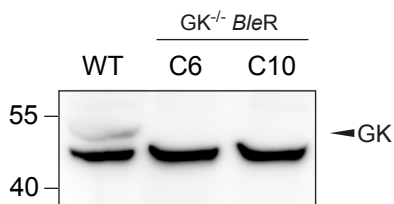
A



B



C



D

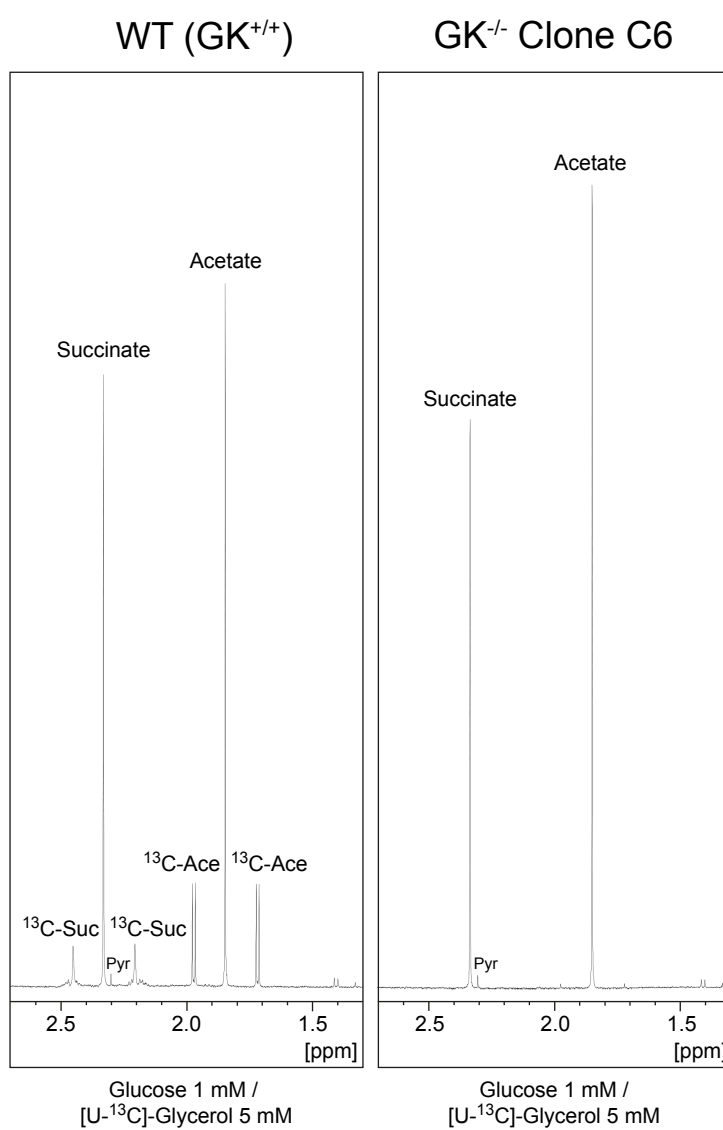


**Figure 6 - Inactivation of the multigenic family encoding the glycerol kinase (GK) in *T. congoense* BSF.** (A) Schematic representation of the GK locus and its inactivation by inserting the phleomycin resistance marker *BleR*. The position of the guide RNA is indicated by a vertical arrow (*TcGK\_1097*) and the 50-bp flanking sequences allowing repair through HDR are shown in gray. (B) PCR confirmation of *GK* gene inactivation on both alleles in two different BSF clones. (C) Western blot analysis of whole-cell extracts from two phleomycin-resistant *T. congoense* BSF clones. (D) <sup>1</sup>H-NMR analysis of end products (succinate and acetate) excreted from the metabolism of glucose and [U-<sup>13</sup>C]-glycerol by the parental (WT) and clone C6 (GK<sup>-/-</sup>) BSF cell lines. A portion of each spectrum ranging from 1.3 ppm to 2.7 ppm is presented. In the NMR experiments, *T. congoense* BSF were incubated in the presence of a mixture of D-glucose (1 mM) and D-[U-<sup>13</sup>C]-glycerol (5 mM) to keep them alive. Resonances were assigned as follows: Ace, acetate; <sup>13</sup>C-Ace, <sup>13</sup>C-enriched acetate; Suc, succinate; <sup>13</sup>C-Suc, <sup>13</sup>C-enriched succinate; Pyr, pyruvate.

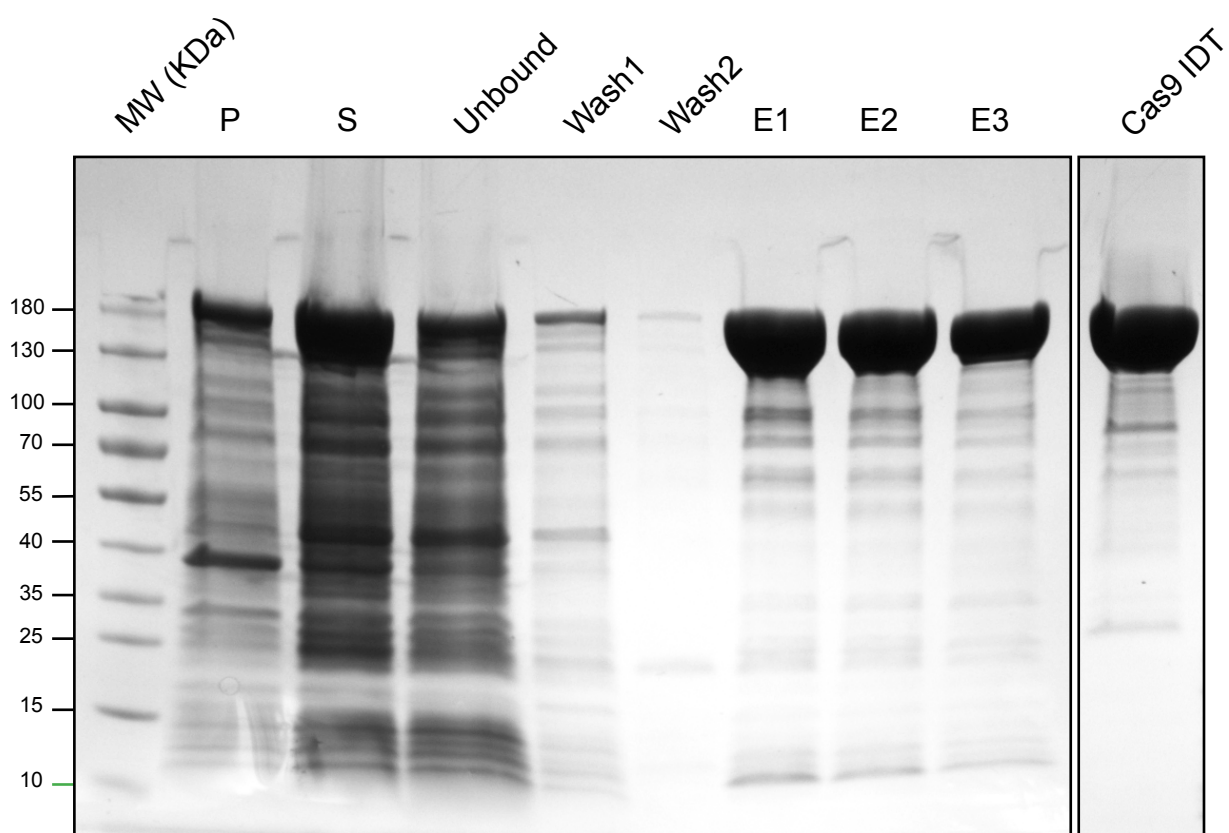


**Figure S1 - Expression and purification of the eSpCas9 from *E. coli*.** The eSpCas9 protein expressed in *E. coli* was purified on a His-Select Nickel column. P, pellet; S, supernatant; Unbound, protein not retained on the column; Wash1 and 2 correspond to the wash fractions; E1 to E3 correspond to the elution fractions. The last lane represents 5  $\mu$ g of purified Cas9 commercially available from IDT.

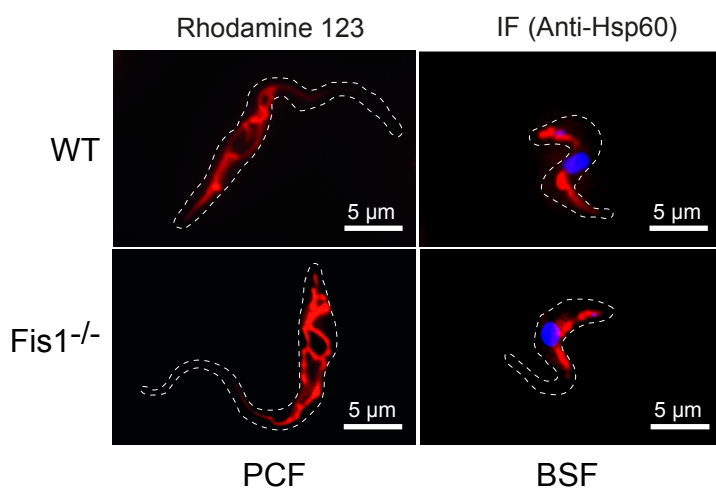
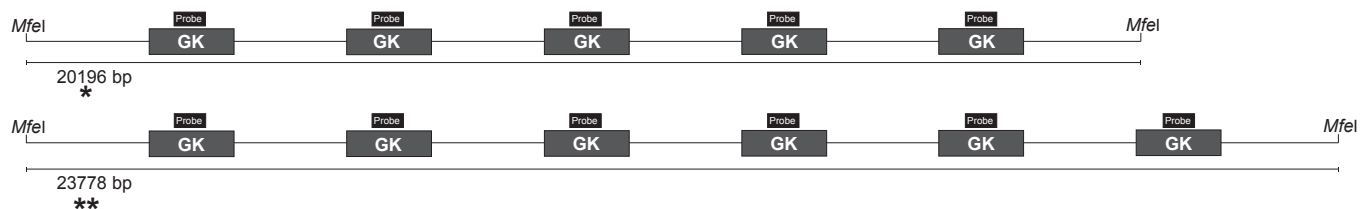


**Figure S2 - Inactivation of the *TbFis1* gene in both *T. brucei* PCF and BSF.** Mitochondrial structure analysis using rhodamine 123 staining on living parental (WT) and *TbFis1*<sup>-/-</sup> PCF cell lines, and with immunofluorescence using an antibody directed against Hsp60 to label and visualize mitochondrial shape in BSF cells. Only the BSF were labeled with DAPI.

**A**



**B**

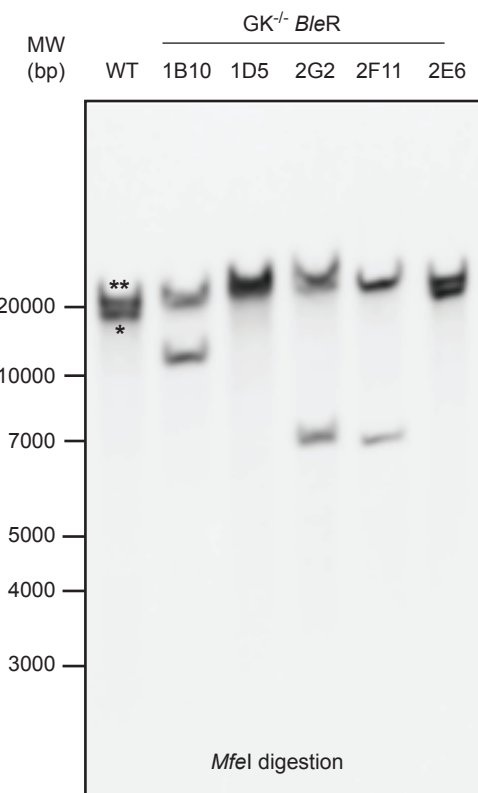


**Figure S3 - Inactivation of the multigenic family encoding the glycerol kinase (GK) in *T. brucei* PCF. (A)** Schematic representation of the two alleles of the *GK* gene cluster in *T. brucei*. The position of the probe used for the Southern-blot analysis is indicated by a black box. **(B)** Southern blot analysis of various phleomycin-resistant clones. Genomic DNA was digested with *MfeI*, separated on a 0.8% agarose gel, transferred to a membrane (Hybond-N), and probed with a PCR product labeled with the PCR DIG Probe Synthesis Kit (Roche). The two bands detected in the parental cell line (WT) correspond to the allele containing 5 (one asterisk) or 6 (two asterisks) copies of the *GK* gene. The insertion of the resistance marker into the various copies of *GK* can either increase the size of the *MfeI* fragment or reduce it if deletion of *GK* copies occurred by homologous recombination after Cas9 cleavage.

723 **SUPPLEMENTAL MATERIAL**

724  
725  
726  
727

**Table S1 - Oligonucleotides used.**

Organism	Gene	Name	Function	Sequence
NA	SV40 NLS	ET20	Third NLS	<b>AAAGGAATTTCGCTAGCGCAGCGGCCGTACCCAAAGAAGAAAGGAAGGTTGACGACGACAACGCTCGAGAAA</b>
		ET21	Third NLS	<b>TTTCTCGAGCTTGTGTCGTCGTCAACCTCCTTTCTCTTGGGTACCGCGCCGCTGCCGCTAGC</b> <b>GAATTCC</b>
NA	GFP	ET18	PCR control	GGGCAGGAACTGTTCACTGGCG
		ET19	PCR control	ATCTTGAAGTGTACCTTGATGCC
<i>T. brucei</i>	FIS1 (Tb927.10.8660)	ET24	PCR control	CGCAAGGTAGCAGGAAAGCTG
		ET25	PCR control	AAATTTAACTACGAAATACGGCC
		ET226	Cassette <i>BleR</i>	GTGTCGGCTCATGGAGTCGCTGGCTTGGCTATGGCAGAGGCGATGG <b>AGCCGTACCGGGGACAGCAAGG</b>
		ET227	Cassette <i>BleR</i>	GGTTCTTCATTTGCGATGCTGCTGGATGGCTGGCTGGGGCTCCCTGCAAGGCCTTGCAAGAAACTGC
		ET255	Cassette <i>SBS</i>	GTGTCGGCTCATGGAGTCGCTTGGCTATGGCAGAGGCGATGG <b>TGATTGATTGAGGATCTGATTGATTGA</b>
		ET256	Cassette <i>SBS</i>	GGTTCTTCATTTGCGATGCTGCTGGATGGCTGGCGTGGGGCTCCCTCAATCAATCAGGATCCTCAATCAAT
	Glycerol Kinase (Tb927.9.12610)	pGK-crispr-ct15'	PCR control	GTCGGATCCATTGACAGGAGA
		pGK-crispr-ct13'	PCR control	ACAATTCAGGAGACCATTTCC
		pGK-BLE-crispr-5'	Cassette <i>BleR</i>	ACGGTGGCTGGGATCGCCTTACCAAGGAACCGCTGTGCTACGCCCTGT <b>CTTGCATGCCGTCAAGGCCTTGCA</b>
		pGK-BLE-crispr-3'	Cassette <i>BleR</i>	AGCTCCGACGGCACCTTCTTGGTGTGCTACGTGCGCAGGTCATTCAACAGGAGATCTAGCCGTACCGGGGC
		pGK-S55	Probe	GTTCCTAACGTTGCGATGCCATGCCCTCGTGGGA
		pGK-S53	Probe	GGGACACTCGAGGCAAACCTCTCACACTCTGTGAT
		ET62	PCR control	GATCCATATGAGCTTGGATCC <b>ATGCTGGTGCCACCCCTC</b> ACTCGC
		ET63	PCR control	GATCGCGGCCGGTACCT <b>CACGGCTGACAATGGGGCCCTTGAG</b>
<i>L. infantum</i>	Aldehyde Dehydrogenase (LINF_250017300)	ET83	Cassette <i>PacR</i>	CGCCGACTTGGAGGAGGGCGCAGGTCGCGCAGACCGGTGTACTTCAT <b>ATGACCGAGTACAAGGCCACGGTG</b>
		ET84	Cassette <i>PacR</i>	AGACTCGTGTACATAAAATGCCGCGACGCCGCGCACCTGGCCGTGTTCAAGGCACGGGCTTGCGGGTCATG
		ET85	Cassette <i>mRED</i>	CGCCGACTTGGAGGAGGGCGCAGGTCGCGACGCCGTTGACTTCAT <b>ATGGCTCCCTCCGAGGACGT</b> CATC
		ET86	Cassette <i>mRED</i>	AGACTCGTGTACATAAAATGCCGCGACGCCGCGCACCTGGCCGTGTTCAAGGCACGGGCTTGAGTGGCGGCC
		ET237	Cassette <i>SBS</i>	CGCCGACTTGGAGGAGGGCGCAGGTCGCGACGCCGTTGACTTCAT <b>TGATTGATTGAGGATCTGATTGATTGA</b>
		ET238	Cassette <i>SBS</i>	AGACTCGTGTACATAAAATGCCGCGACGCCGCGCACCTGGCCGTGTTCAATCAAT <b>CAGGATCCTCAATCAATCA</b>
		ET261	PCR control	GGAACTCGGTAACGACCAAAG
		ET262	PCR control	CATCAGCAGGCCAAGGTAGC
<i>T. congolense</i>	LysoPLA (TcIL3000_A.H_000623300)	ET298	Cassette <i>BleR</i>	ATGGTGGCATGACGATGAATTCTGGTACGACATAAGGGACGGGACCTT <b>AGCCGTACCGGGGACAGCAAGG</b>
		ET299	Cassette <i>BleR</i>	GGTAGTCGCTGACTTCATAATGGTTCTGGTCCCTCACGTTCCCTCACCTGCAAGGCCTTGCAAGAAACTGC
		ET358	Cassette <i>SBS</i>	AAATGGTGGCATGACGATGAATTCTGGTACGACATAAGGGACGGGACCTT <b>TGATTGATTGAGGATCTGATTGA</b>
		ET359	Cassette <i>SBS</i>	GGTAGTCGCTGACTTCATAATGGTTCTGGTCCCTCACGTTCCCTCAC <b>TCAATCAATCAGGATCCTCAATCAATCA</b>
		ET263	PCR control	CCTTGCCTACGCTCTCGAG
		ET264	PCR control	CAAGGGATGTCACACCCAGTAGG
	Glycerol kinase (TcIL3000_0_55170)	ET296	Cassette <i>BleR</i>	TCGTTCCCGCCTCTCCGGCTGCTGGCGCCATTGGGACCCCTGGCT <b>AGCCGTACCGGGGACAGCAAGG</b>
		ET297	Cassette <i>BleR</i>	ATGATATGTCGCGCTGTCGCTTAACGCTCATCCGACGATGGTCCACGGCCTG <b>CTGCAAGGCCTTGCAAGAAACTGC</b>

**Table S2 – Guides RNA used.**

Organism	Gene	Guide name	Sequence (PAM)
NA	Green Fluorescent Protein	GFP1/GFP_97	GGTGAAGGTGATGCCACATA(CGG)
		GFP2/GFP_150_revcom	AGTGGTGCAGATGAATTCA(GGG)
		GFP3/GFP_336	CAAGTTCGAAGGTGACACCC(TGG)
<i>T. brucei</i>	Fis1	TbFIS1_248	TATGGCAGAGGCGATGGGA(GGG)
<i>T. brucei</i>	Glycerol Kinase (GK)	GK_325rc	TGCGCAGGTCTCCAAACA(GGG)
<i>L. infantum</i>	Aldehyde Dehydrogenase (ALDH)	ALDH_864	GACCGGTGCTACTTCACAA(CGG)
<i>T. congolense</i>	LysoPLA	TcPLA_370	ATAAGGGACGGGACCTTGA(AGG)
<i>T. congolense</i>	Glycerol Kinase (GK)	TcGK_1097	ATTGGGACCCCTGGCTCGT(GGG)

728  
729  
730  
731  
732

733  
734  
735  
736  
737  
738